ANTARCTIC SEA ICE: PHYSICAL PROCESSES, INTERACTIONS AND VARIABILITY
ANTARCTIC RESEARCH SERIES, VOLUME 74, PAGES 243-271

ANTARCTIC OCEAN-ICE INTERACTION: IMPLICATIONS FROM OCEAN BULK PROPERTY DISTRIBUTIONS IN THE WEDDELL GYRE

Douglas G. Martinson and Richard A. Iannuzzi

Lamont-Doherty Earth Observatory and Department of Earth and Environmental Sciences, Columbia University Palisades, NY

The sea ice distribution in the Antarctic polar oceans is intimately tied to the underlying ocean structure, which controls the oceans' vertical heat flux and stability. The former determines the rate at which ice grows for a given air-sea heat flux, while the latter limits the amount of sea ice that can grow locally before overturning the water column. These relationships have been described through a set of scalings, allowing us to estimate, through examination of the vertical distributions of ocean temperature and salinity: (1) the maximum amount of *in situ* ice growth in any one location, (2) the ratio of ice melt to ice growth, (3) the amount of ice that has melted in any particular summer location, (4) the ocean winter-averaged heat flux. Climatological maps of these quantities are presented for the Weddell gyre region and general results described. Results include: (1) the sea ice cover throughout the seasonal sea ice region is typically 0.6 m thick or less by the spring melt period, though it is thinner than 0.3 m in some regions near the gyre core; (2) the ocean-ice system manages to liberate heat from the deep water at an average winter rate of 25-35 W m^{-2} throughout the gyre, regardless of the large scale stratification and dynamic setting which reflect different processes by which the heat makes its way to the surface from the deep waters; (3) strong mixing due to the passage of intense polar lows may serve to reduce the bulk stability of the water column by as much as 75%; (4) most of the bulk stability of the water column is attributed to the enthalpy content of the thermocline, not by direct reduction in ice growth by a strong diffusive heat flux; and (5) positive perturbations (i.e., excess ice growth) in the annual *in situ* ice growth of $\geq$80% are required to overturn the water column throughout much of the Weddell gyre. The bulk parameters presented here involve vertically-integrated property distributions, and as such they provide constraints or limitations on the ocean-ice system behavior over seasonal time scales. Consequently, they imply a mean seasonal evolution which may be considerably different from the actual time-dependent behavior.

1. INTRODUCTION

Numerous studies have suggested that the polar oceans play an important role in global climate over a broad range of time scales [e.g., *Washington and Meehl*, 1984; *Hanson et al.*, 1984; *Schlesinger and Mitchell*, 1985; *Meehl and Washington*, 1990; *Manabe et al.*, 1991; *Ledley*, 1991; *Imbrie et al.*, 1992; *Wadhams*, 1994; *Rind et al.*, 1995]. In the marginally stable Antarctic polar oceans, the sea ice distribution, ocean heat flux and ocean stability represent three fundamentally important components of this coupled polar-climate system. The sea ice distribution modulates climate through its insulating effect, high albedo and freshwater transport. The latter influences ocean stability and ventilation of deep waters. The ocean heat flux directly influences

the rates of ice growth and deep water ventilation. The stability controls the likelihood of a system mode change [e.g., *Gordon*, 1991] from its current semi-stable mode, which supports a seasonal sea ice cover with coastal deep-water formation, to an unstable mode with open ocean deep water formation and the inability to support a sea ice cover. The Weddell polynya was the signature of the most conspicuous example of the unstable mode on a regional scale [*Gordon*, 1978; *Killworth*, 1979; *Martinson et al.*, 1981; *Parkinson*, 1983; *Motoi et al.*, 1987; *Walin*, 1993].

Given the climatic relevance of the sea ice distribution, ocean heat flux and ocean stability, the purpose of this paper is to present a set of parameters, derived from easily observed features of the water column, that impose controls or limitations on these 3 characteristics. The ability to do this reflects the fact that the ocean-atmosphere-ice (OAI) system is so highly interactive that a change in one part of the system influences all other parts. Since the ocean structure has the longest integrated-property memory within the seasonal OAI system, it can be examined anytime within a year and still provide the relevant information [e.g., *Gordon*, 1981]. Ocean properties thus provide an ideal component for use in establishing such parameters. Also, since the sea ice spatial distribution is the most easily observed polar characteristic (from space), the parameters are presented so as to provide information regarding that component of the sea ice distribution which is most difficult to obtain: sea ice thickness.

Specifically, through examination of the vertical distributions of ocean temperature (T) and salinity (S), we estimate: (1) sea ice growth and thickness constraints, (2) winter mean contributions of the ocean heat flux, and (3) susceptibility to deep convection (i.e., overturning the water column, ice elimination and mode change). Time-averaged (climatology) spatial distributions of the parameter values within the Weddell gyre are then provided to demonstrate their usefulness and interpretation, though the concepts apply to anywhere within the sea ice fields. The benefits of such parameters lie in their ability to easily encapsulate fundamental seasonally-averaged characteristics of the OAI system and their sensitivities, and present them in a manner amenable for evaluation of their spatial and temporal variations. They are not appropriate for estimating detailed time-dependent behavior, which may deviate significantly at any one time from the predicted mean evolution presented here.

2. CONCEPTS

To estimate the OAI system parameters of interest based on critical features of the upper water column requires knowledge of the system's external parameter dependence. This was developed for the winter season by *Martinson* [1990], in which a linear system was reduced to a set of simple scaling relationships that captured most (≥83%) of the variance of the full linear model (the implications and deficiencies of a linear treatment are evaluated below). These relationships provide prognostic estimates of ice thickness, mixed layer entrainment (destabilization), and mixed layer salinity as a function of the external parameters of the system: mixed layer and pycnocline thicknesses; T and S gradients (∇T, ∇S) through the pycnocline; the external surface forcing (heat and freshwater); and, diffusive mixing across the pycnocline. The latter is represented, for lack of a better parameterization, by a turbulent diffusivity coefficient. The scalings and diagnostic relationships revealing their inter-dependencies, establish the foundation from which parameters relating the ocean features to ice thickness, ocean heat flux and bulk stability are defined here.

A fundamental, though non-limiting, assumption in the use of these scalings and related parameters is that the OAI system is predominantly controlled by vertical processes. This assumption should be fairly reasonable throughout most of the Weddell gyre, as evidenced by relatively weak (in the mean) lateral property gradients [e.g., *Gordon and Molinelli*, 1982; *Bagriantsev et al.*, 1989], away from the gyre boundaries and the predominant topographic feature, Maud Rise at 1° E and 67° S. Where the assumption is violated, that is, where lateral fluxes contribute significantly to the local evolution of the surface water column, the scalings, and integrated (bulk) parameters presented here will still represent valid approximations if spatially averaged over scales comparable to those representing the range of influence of the lateral fluxes over the length of a season (the integration time of the parameters). This averaging is introduced when producing the climatological maps of Section 4.

Where spatial averaging does not properly accommodate lateral fluxes is in the vicinity of the continental margins where new water masses are being formed, and thus their properties are not accounted for in the integrated ocean profiles. Since these new water masses typically exit the surface layer by flowing along the continental margins [e.g., *Foldvik and Gammelsrød*, 1988; *Gordon et al.*, 1993], the regions for which the parame-

ters are invalid should mainly be constrained to the region of the continental shelf. The depth contour delimiting this region, at approximately 1000 m depth, is outlined in the parameter maps presented later, and provides an approximate southern limit to the parameter validity.

Other basic assumptions in this linear system are that the upper ocean property profiles must display the general shapes shown in Figure 1, and the surface forcing is assumed to be smooth — that is, constant or slowly varying within a season relative to the time constants of the OAI system. Significant departures from the general profile shapes are unacceptable; in such cases, the profiles are excluded from the analysis as discussed in Section 3. Violation of the smooth forcing is more difficult to anticipate, but attempts to do so are considered later in this section.

Linear Winter System: Primary Parameters

Winter salt deficit (SD_w) and thermal barrier (TB_w). In essence, much of the oceanic control on the ice thickness, ocean bulk stability and heat flux, revolves around the distribution of heat and salt within the mixed layer and pycnocline. Specifically, as defined in *Martinson* [1990], the relationship between the winter "thermal barrier" (TB_w) and "salt deficit" ($_{SD_W}$), both described below, dictates a considerable amount of the system evolution and control. The term "winter", as used here, is that period of the year for which the T and S profiles display the general form of Figure 1a. That is, the surface layer does not contain a seasonal pycnocline; the surface mixed layer is more or less in direct contact with the permanent pycnocline.

The total winter salt deficit, SD_w^T is the stabilizing

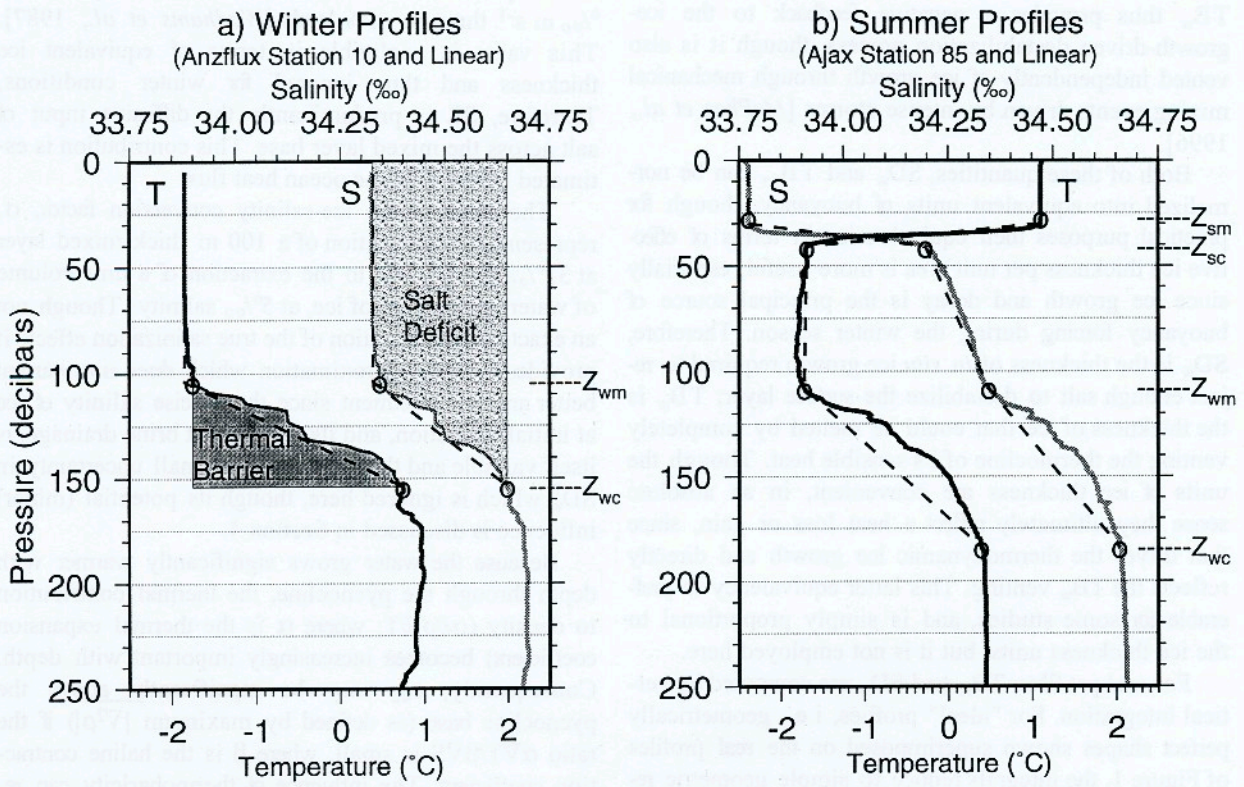

Figure 1: Ideal winter (a) and summer (b) profiles of T and S. Dashed line shows ideal profile shapes; shading indicates the area integrated to produce the Thermal Barrier and Salt Deficit for winter profiles. Key integration depths referred to in the text are also indicated.

freshwater content of the winter mixed layer, relative to the salinity near the base of the pycnocline, that must be eliminated in order to destabilize the surface layer, overturning the water column and driving deep convection. Some of this salt is supplied by the deep ocean, via turbulent diffusion and entrainment. An estimate of this ocean contribution can be removed leaving the corrected winter salt deficit, SD_w (hereafter referred to simply as winter salt deficit), that must be eliminated predominantly by salt rejection driven by ice growth.

TB_w is the sensible heat (enthalpy in excess of the freezing point, T_f) available in the thermocline that must be vented by erosion of the pycnocline during destabilization. As it is vented, that is, mixed into the surface layer, this enthalpy effectively stabilizes the water column by melting ice or, equivalently, by preventing ice growth which would otherwise destabilize through salt rejection. Therefore, as the SD_w is reduced by salinization during ice growth, static instability drives entrainment that gradually vents the TB_w, freshening the surface layer and restabilizing it to some degree. The TB_w thus provides a negative feedback to the ice-growth-driven destabilization process, though it is also vented independently of ice growth through mechanical mixing events driven by intense storms [*McPhee et al.*, 1996].

Both of these quantities, SD_w and TB_w, can be normalized into equivalent units of buoyancy, though for practical purposes their equivalencies in terms of effective ice thickness per unit area is more useful, especially since ice growth and decay is the principal source of buoyancy forcing during the winter season. Therefore, SD_w is the thickness of *in situ* ice growth required to reject enough salt to destabilize the surface layer; TB_w is the thickness of ice that could be melted by completely venting the thermocline of its sensible heat. Though the units of ice thickness are convenient, in an absolute sense they ultimately reflect a heat loss or gain, since that drives the thermodynamic ice growth and directly reflects the TB_w venting. This latter equivalency is preferable for some studies, and is simply proportional to the ice thickness units, but it is not employed here.

For real profiles, TB_w and SD_w are computed by vertical integration. For "ideal" profiles, i.e., geometrically perfect shapes shown superimposed on the real profiles of Figure 1, the integrals reduce to simple geometric relationships:

$$TB_w = [(T_{wp} - T_f)h_{wp}/2](\rho_w c_w/\rho_i L_i) \quad (1)$$

and

$$SD_w^T = (S_{wp} - S_{wm})(h_{wm} + h_{wp}/2)\sigma^{-1} \quad (2a)$$

$$SD_w = SD_w^T - SE \quad (2b)$$

where: T_{wp} and S_{wp} are T and S at z_{wc}, the critical depth near the base of the winter (permanent) pycnocline, below which additional entrainment occurs via cooling alone (i.e., no additional salinization is required for further destabilization once entrainment mixes down to this depth); h_{wp} is the thickness of the winter pycnocline to the critical depth; ρ_w and ρ_i are the densities of water and sea ice, respectively; c_w is the specific heat of seawater; L_i is the latent heat of fusion of sea ice; S_{wm} is the salinity of the winter mixed layer; h_{wm} is the thickness of the winter mixed layer; and σ (= 30‰) is a convenient means of converting a unit of ice to an ocean mixed layer salinity increase. SE is the net contribution of salt from other non-ice sources, such as eddy diffusion across the base of the mixed layer and freshwater input at the surface due to snow entering through leads. Winter snow input is estimated from *Martinson* [1990] as ~10^{-9} ‰ m s^{-1} through ~5% leads [*Wadhams et al.*, 1987]. This value is negligible in terms of equivalent ice thickness and thus ignored for winter conditions. Therefore, SE is predominantly the diffusive input of salt across the mixed layer base. This contribution is estimated below with the ocean heat flux.

The value of the ice-salinity conversion factor, σ, represents the salinization of a 100 m thick mixed layer at 35‰ salinity due to the extraction of a unit volume of water, in the form of ice, at 5‰ salinity. Though not an exact parameterization of the true salinization effect, it provides a close approximation which does not warrant better analytic treatment since the precise salinity of ice at initial formation, and its subsequent brine drainage, is itself variable and thus represents a small uncertainty in SD_w^T which is ignored here, though its potential (minor) influence is discussed in Section 4.

Because the water grows significantly warmer with depth through the pycnocline, the thermal contribution to density ($\alpha\partial\rho/\partial T$; where α is the thermal expansion coefficient) becomes increasingly important with depth. Consequently, z_{wc} may be significantly above the pycnocline base (as defined by maximum $|\nabla^2\rho|$) if the ratio $\alpha\nabla T/\beta\nabla S$ is small, where β is the haline contraction coefficient. The influence of thermobaricity can reduce z_{wc} further (e.g., *Garwood et al.*, 1994; *Akitomo et al.*, 1995) though it is not considered here.

In isolation, SD_w indicates the overall degree of stability in the water column associated with the surface freshwater cap, while TB_w indicates the potential to re-

sist overturn due to the heat storage in the thermocline. In various combinations these fundamental parameters provide the basis for several more quantities of interest.

Bulk stability. The most notable combination of SD_w and TB_w occurs in the form of net surface water, or bulk, stability (Σ), where $\Sigma = TB_w + SD_w$. This measure of stability indicates the amount of *in situ* ice growth (or its heat loss equivalent) sufficient to overturn the water column and drive deep convection, ignoring storm influences or thermobaric effects, both discussed later.

Bulk stability is the sum of both SD_w and TB_w because the destabilization induced by growing an amount of ice equivalent to SD_w will completely eliminate the thermocline, melting or preventing the growth of an amount of ice equivalent to TB_w. Thus, an additional amount of ice equal to TB_w must then grow in order to overcome the freshwater introduced by the melt (or its effective freshening by the prevention of ice growth). This value is an upper limit since storms can effectively reduce its influence on the ice budget, as discussed later.

Diffusive heat flux. The ability of the water column to resist destabilization by ice growth lies in the ocean heat flux; that is, the transfer of heat from the warm deep water into the mixed layer (by entrainment), reduces ice growth. Turbulent diffusion accomplishes this directly by mixing the warm deep water upward, which continually decreases the density stratification at the base of the mixed layer, making it possible to mix this weakly stratified warmer water into the mixed layer without a change in surface mixing intensity. Therefore, on average, turbulent diffusion directly effects a heat flux into the mixed layer, without the need to explicitly account for the entrainment process (i.e., the background mixing in the mixed layer is sufficient).

The direct contribution of ocean sensible heat via turbulent diffusion across the pycnocline (F_{DT}), preventing a destabilizing ice growth, is given as $F_{DT} \approx \rho_w c_w K_z \nabla T$, where all quantities here (and in following definitions) are for seasonally-averaged values unless otherwise noted; K_z is an eddy diffusivity coefficient. Results of the recent ANZFLUX experiment [*McPhee et al.*, 1996] reveals that K_z changes significantly with the intensity of the surface stress forcing [*Stanton*, personal communication]. Thus, it is difficult to assign a single constant value for K_z. On the other hand, property distributions [e.g., *Gordon and Huber*, 1990; *Schlosser et al.*, 1987] and simple modeling studies [e.g., *Martinson*, 1990] suggest that a seasonally-averaged value, $K_z \sim 0.6 \times 10^{-4}$, is required to achieve the observed seasonal heat balance. This value is large [e.g., *Gregg*, 1988, *Ledwell*, 1993], but apparently reflects the tremendous episodic increase in turbulent diffusion during the frequent storm events, as suggested by the ANZFLUX experiment. It may also reflect the weak stratification of the Antarctic pycnocline. Regardless, this is approximately the average winter value required to achieve the observed average seasonal heat flux estimated in a number of previous studies, referenced above. The impact of using a single, invariant value for K_z is discussed in Section 4 when discussing the results. Note that the dependency of K_z on the surface stress suggests that during summer, when the permanent pycnocline is isolated from this stress by the seasonal pycnocline, that the average value of K_z will be small, which is consistent with the fact that the remnant winter mixed layer survives relatively intact through the summer months.

As an ice-melt, or ice-growth-inhibitor, potential, this turbulent-diffusive heat flux can be provided in terms of equivalent ice thickness: $\Theta_{DT} = F_{DT}\Delta t/\rho_i L_i$, where Δt is the time period (~5 months) over which the ocean is in its winter configuration (i.e., with the deep winter mixed layer present). This provides an estimate of the thickness of ice that is prohibited from growing, or is actively melted, by this heat flux component.

Entrainment heat flux. Whereas the turbulent diffusive flux directly resists destabilization by reducing ice growth by an amount Θ_{DT}, any net ice growth that is realized must salinate the mixed layer, driving static instability and a density adjustment through free convection. The free convection, or entrainment, erodes the thermocline, releasing heat stored in the thermal barrier, venting TB_w as the negative feedback mechanism previously discussed.

In the context of the water column's ability to resist overturning, this entrainment heat flux is most effectively presented as a *TB_w efficiency ratio*: $\gamma_{TB} \approx TB_w/\Sigma$. This ratio provides an indication of the overall fraction of bulk stability attributed to the thermal barrier, or negative feedback. Where the value is large (approaching 1), the bulk stability is dominated by the large enthalpy content of the thermocline; where it is small, the surface freshwater content dominates. This differentiates between subsurface versus surface stabilization. The latter reflects stability largely attributed to ice drift which controls the surface freshwater balance, while the former reflects stability due to enthalpy contained within the thermocline. Both sources are linked through the larger scale surface stress forcing.

As a heat flux potential, γ_{TB} represents the percent of the air-sea heat flux provided initially as latent heat of fusion (i.e., the net air-sea heat flux minus F_{DT}) that will ultimately be realized as an ocean sensible heat flux. For

example, if $\gamma_{TB} = 0.2$, $F_{DT} = 20$ W m^{-2} and the average air-sea heat flux, $F_a = 35$ W m^{-2}, then 15 W m^{-2} must initially be provided to the atmosphere as latent heat of fusion, F_{LT}, or $F_{LT} = F_a - F_{DT}$. This grows enough ice to drive an entrainment heat flux (i.e., venting of TB_w), $F_{ET} = \gamma_{TB} F_{LT} = 0.2 \times 15 = 3$ W m^{-2} of sensible heat from the TB_w; or, given as an equivalent ice-growth-inhibitor potential: $\Theta_{ET} = F_{ET}\Delta t/\rho_i L_i$. Therefore, the net ocean sensible heat flux is the diffusive plus entrainment fluxes, or $F_T = F_{DT} + F_{ET} = 23$ W m^{-2}. This net value can be given as a total ice-growth-inhibitor: $\Theta_T = F_T \Delta t/\rho_i L_i$. Alternatively, 20% ($\gamma_{TB} = 0.2$) of every watt of heat released to the atmosphere as latent heat of fusion (ice growth) is ultimately converted, through the negative feedback, to a sensible heat flux. Thus, γ_{TB} indicates the efficiency of the negative feedback mechanism in extracting additional ocean sensible heat (TB_w-ventilation) from the subsurface waters that is otherwise not directly accessible to the surface. In a seasonal bulk analysis, this ratio is arguably more important than the average entrainment heat flux, as it gives a direct indication of the relative importance of the thermal barrier in maintaining the water column stability, and thus some indication of the mechanistic controls, and relative sensitivities, of the system.

Linear Winter System: Additional Diagnostic Parameters

Ice melt to growth ratio. Another measure of the efficiency of the negative feedback is given by the ratio $\gamma_\Theta = TB_w/SD_w$. This ratio indicates the effectiveness of the feedback mechanism in melting or inhibiting ice growth. For each unit of ice growth (destabilization), γ_Θ-units of ice melt (stabilization) are introduced by the venting of the TB_w. Thus γ_Θ is the ratio of *in situ* melt to growth. If $\gamma_\Theta > 1$, for each unit of ice grown, more than one unit of ice melts, resulting in a significant reduction in the net growth rate.

For example, if $\gamma_\Theta = 9$, and one unit of ice grows per day, then one day's growth vents enough of the TB_w to prohibit ice formation for the next 9 days, or it melts 9 units of ice immediately, requiring the next 9 days to regrow the melted ice and overcome the 9 units of stabilizing meltwater. In a 10-day period, net ice growth occurs for only 1 day so a growth efficiency is defined as $\gamma_{SD} = (\gamma_\Theta + 1)^{-1} = SD_w/\Sigma$. This is the salt deficit equivalent to γ_{TB}. It controls the *effective* latent heat flux required to make a net reduction in the stability. The effective latent heat flux, $\langle F_{LT}^{eff} \rangle = \gamma_{SD} \langle F_{LT} \rangle$, gives the latent heat flux resulting in the net increase in ice after compensating for ice melt due to TB_w venting. So, $\langle F_{ET} \rangle + \langle F_{LT}^{eff} \rangle = (\gamma_{SD} + \gamma_{TB}) \langle F_{LT} \rangle = \langle F_{LT} \rangle$, the original (gross) latent heat flux, of which some fraction, γ_{TB}, is converted to a sensible heat flux via venting of the TB_w, melting ice, while the complement goes toward the actual net increase in ice thickness. Also, $\gamma_\Theta = \gamma_{TB}/\gamma_{SD}$.

Ocean heat flux distribution. The ocean heat flux, as partitioned here, is realized through the eddy-diffusive flux, F_{DT}, and entrainment-driven flux, F_{ET} [for a more complete discussion of the ocean heat flux dependencies, relative contributions and sensitivities to diffusion, upwelling and free/forced convective entrainment on the ocean heat flux, see *Martinson*, 1990, 1993]. The diffusive flux draws heat directly from the deep water, a near infinite reservoir, while the entrainment flux taps the finite reservoir stored within the thermocline. This separation is artificial since entrainment is required to incorporate all warmer water into the mixed layer, and the ultimate source of the enthalpy comes from the deep water in each case. However, it represents a rather natural separation reflecting the processes and time scales of the different mechanisms by which heat is transferred to the surface. Upwelling and other gyre-scale dynamics also influence this categorization, though these are treated through their influence on the mixed layer depth and pycnocline characteristics, which control the bulk parameterizations. In any case, the ratio of these two seasonally-averaged fluxes, or their ice-melt equivalencies, $\gamma_T = \Theta_{ET}/\Theta_{DT}$, provides an indication of the immediate source of the ocean heat.

For small values of γ_T, the ocean heat flux is dominated by the diffusive flux; for large values the entrainment flux dominates. The primary control on this ratio is the thickness of the thermocline, since, for a given T_{max} at the base of the thermocline (i.e., for a given deep water T), this thickness controls both ∇T (dominating F_{DT}) and TB_w (dominating F_{ET}). The explicit (bulk) covariation between F_{DT} and F_{ET} can be determined analytically, but the result is algebraically tedious and not particularly insightful. In essence, small ratios of γ_T reveal areas where deep water enthalpy is most effectively vented directly across a thin thermocline that provides little thermal storage itself. Large values reflect a deep water that is more effectively buffered by a thick thermocline that undermines diffusion but which stores considerable enthalpy that is vented via entrainment.

The thin pycnocline reflects: (1) a stronger upwelling, effectively forcing the deep water closer to the surface layer, and/or (2) a greater mean surface stress, or greater frequency/intensity of storms, that increase the

depth of the surface layer, effectively forcing it closer to the deeper water. Both scenarios allow a more direct interaction between the deep water and surface layer. Conversely, the thick pycnocline indicates the opposite, and the interaction between the surface and deep waters must be effected through an intermediate process, entrainment. However, either situation allows the atmosphere access to the deeper ocean sensible heat it ultimately requires.

The relative heat flux contributions can also be given as $\Gamma_{ET} = \Theta_{ET}/(\Theta_{ET} + \Theta_{DT})$ and $\Gamma_{DT} = \Theta_{DT}/(\Theta_{ET} + \Theta_{DT})$. These ratios provide the fraction of the total heat flux (or ice-growth inhibition) contributed by the entrainment-driven, or diffusive components, respectively.

Salt flux distribution. An eddy diffusive flux for salt, F_{DS}, is estimated by: $F_{DS} \approx K_z \nabla S$. Like the eddy diffusive heat flux, it too can be given in terms of equivalent units of ice, $\Theta_{DS} = F_{DS}\Delta t/\sigma$, representing the ice growth required to contribute this degree of salinization. Also, a ratio relates the sources of salt, $\gamma_S = SD_w/SE$, where $SE \approx \Theta_{DS} + \Theta_{ES}$, and Θ_{DS} is the diffusive contribution as defined previously and Θ_{ES} is the contribution of excess salt as the halocline is mixed into the surface layer via entrainment. This ratio indicates how much of the destabilization, measured as the elimination of the total salt deficit, SD_w^T, is contributed by deep ocean salt sources relative to that which must come from surface freshwater extraction (ice growth). Large values of γ_S indicate that the predominant source of salt must be forced by heat loss driving ice growth.

Since Θ_{ES} is driven by a latent heat flux through the negative feedback mechanism, ice growth is ultimately responsible for reducing SD_w^T by both SD_w (salinization by ice) and Θ_{ES} (direct consequence of the salinization). Thus, the salt ratio can be defined in terms of the forcing, rather than sources, of salt: $\gamma_{Si} = (SD_w+\Theta_{ES})/\Theta_{DS}$, where γ_{Si} is a measure of the salt deficit reduction by latent heat loss relative to that by ocean diffusion.

The relative salt contributions can also be given as: $\Gamma_{ST} = SD_w/SD_w^T$, $\Gamma_{SS} = SE/SD_w^T$ and $\Gamma_{Si} = (SD_w+\Theta_{ES})/SD_w^T$. These provide the fraction of the total salt deficit that must be contributed by ice growth, ocean salt sources, and latent heat loss, respectively.

Linear Summer System: Primary Parameters

In addition to the winter parameters, the presence of the seasonal pycnocline in the summer provides an opportunity for additional quantities involving the surface layer that is warm and fresh, representing the spring meltwater and summer warming. In these cases the permanent pycnocline features are preserved at depth, though slightly diffused, still allowing computation of the winter parameters just described as well.

Summer salt deficit and thermal barrier. As with winter, the freshwater and thermal content associated with the seasonal mixed layer and pycnocline can be classified in terms of a summer salt deficit, SD_s, and thermal barrier, TB_s. The SD_s in this case is the freshwater content of the summer surface layer relative to the salinity of the remnant winter mixed layer below the seasonal pycnocline. The TB_s, unlike TB_w, is predominantly contained within the surface mixed layer, since temperature decreases through the seasonal thermocline reflecting a diminishing enthalpy content with depth. Consequently, most of this heat is vented via direct exchange with the atmosphere and its primary role is not as a negative feedback inhibiting ice growth, but rather as a thermal buffer that must be eliminated before ice can grow at all. Thus, its main influence is on the seasonality of the ice, and only through that influence can it affect ice thickness (some of the heat is indeed vented by ice growth destroying the seasonal thermocline, but this is a relatively minor fraction). Consequently, it is not sensible to present TB_s in terms of equivalent ice thickness. It is given as enthalpy relative to freezing, though SD_s is still given as equivalent ice thickness.

Consistent with the winter parameters, TB_s and SD_s are computed by vertical integration for real profiles. For ideal summer profiles (Figure 1b), the integrals again reduce to simple geometric relationships:

$$TB_s = [(T_{sm} - T_{min})(h_{sm} + h_{sp}/2) + (T_{min} - T_f)(z_{sc} + h_{wr})]\rho_w c_w \quad (3)$$

and

$$SD_s = (S_{wr} - S_{sm})(h_{sm} + h_{sp}/2)\sigma^{-1} \quad (4)$$

where: T_{sm} and S_{sm} are T and S within the summer mixed layer; h_{sm} is the thickness of the summer mixed layer; h_{sp} is the thickness of the seasonal pycnocline; T_{min} is the minimum temperature, which lies within the remnant winter mixed layer between the seasonal and permanent pycnoclines; z_{sc} is the depth at the base of the seasonal pycnocline (and top of the remnant winter mixed layer); h_{wr} is the thickness of the remnant winter mixed layer; and S_{wr} is the average S of the remnant winter mixed layer.

The second term on the right-hand-side of (3) is broken into two components: the enthalpy content to the

base of the seasonal pycnocline, and then through the remnant winter mixed layer. The former is predominantly vented prior to ice growth, whereas the latter, a relatively small amount, is vented by mixing during removal of the seasonal halocline with the initial ice growth. This latter component does not contribute to the seasonality of the ice cover, but does introduce a slight temporary reduction in initial growth rate during the fall.

SD_s does not have a correction term, corresponding to SE in (2b), since elimination of SD_s during fall ice growth is too fast for diffusion to influence it. The fall ice growth is rapid because: (1) it does not begin until TB_s is vented, eliminating the seasonal thermocline and thus any potential summer negative feedback comparable to that in the winter; (2) the seasonal halocline isolates the surface layer from the deeper ocean heat flux associated with the permanent pycnocline, so there is no inhibiting ocean heat flux, either diffusive or via the deeper negative feedback, save the minor amount $(T_{min} - T_f)h_{wf}\rho_w c_w$; and (3) there is no insulating ice cover to restrict the air-sea heat flux initially. Consequently, the ice grows very rapidly until SD_s is eliminated (along with the seasonal halocline/pycnocline), after which the winter mixed layer is fully developed and in direct contact with the permanent pycnocline, making available the diffusive and entrainment heat fluxes and greatly inhibiting further (i.e., winter) ice growth.

SD_s is dominated by the ice and snow melt from the previous winter as well as runoff, summer precipitation-evaporation and diffusion across the seasonal halocline. Contributions from the latter three are presumably quite small [e.g., *Jacobs et al.*, 1992; *Martinson et al.*, 1981; *Martinson*, 1990] so SD_s is predominantly a meltwater signal. Regardless of the source of freshwater, SD_s represents the thickness of the fall ice growth that will grow rapidly until the winter mixed layer is developed initiating the ocean heat flux influence.

TB_s is of questionable value without specific information regarding the fall air-sea heat flux. For an approximate fall regional heat flux curve, TB_s can be presented as the amount of time until initial ice growth following the onset of fall cooling. However, the fall air-sea heat flux can show tremendous variability in the absence of an insulating ice cover, introducing unacceptably large errors relative to the signal. Alternatively, since satellite coverage reveals the time of initial ice growth, TB_s, in conjunction with the climatological average of when fall cooling begins, allows an estimate of the average fall air-sea heat flux and thus its spatial distribution. However, here too, given the dramatic increase in heat loss later in the fall and potential errors in initiation of fall cooling, such estimates may also be of questionable value.

Linear Summer System: Additional Diagnostic Parameters

Critical interannual ice growth perturbation. The total amount of stabilizing freshwater contained above the permanent pycnocline that must be eliminated, via ice growth, in order to destabilize the water column is given by the sum of the summer salt deficit and winter stability, $\Sigma_T = SD_s + \Sigma$. The fraction of this realized through the fall ice growth is $\gamma_{ms} = SD_s/\Sigma_T$. Since SD_s is predominantly a measure of the spring ice and snow melt, this ratio provides an indication of what fraction of the net stabilizing surface freshwater content is mobile each year through actual ice *in situ* growth/decay, ice divergence/convergence, and snow accumulation. For fractions approaching 1, a relatively small change in ice growth/decay, divergence/convergence, or winter snow accumulation, relative to the seasonal average, may lead to destabilization.

For example, if $\gamma_{ms} = 0.9$, then 90% of the destabilization required to overturn the water column is achieved in a typical year. Conversely, the fraction $\Gamma_{ms} = 1/\gamma_{ms}$ indicates the size perturbation in annual ice thickness relative to the climatological mean required to destabilize the water column. For the above example, a perturbation of ~11% would be sufficient to destabilize the (climatological) water column. Therefore, this parameter can identify regions most susceptible to overturn given interannual variability. In fact, given an estimate of interannual variability at any given location, one can estimate the likelihood of achieving a critical perturbation sufficient to destabilize the water column and induce a mode change. This interpretation is only approximate however, since divergence and ice drift assures that ice does not melt where it forms and thus the actual *in situ* melt may not be indicative of the *in situ* ice growth in that same location.

Nonlinear System

The linear summer and winter descriptions above suffer from several weaknesses. The most conspicuous ones are associated with the assumptions of general profile shapes and a steady surface stress forcing. The former influences the manner in which the parameters are computed as well as the uncertainties associated with their bulk (ideal-geometry) calculation, though this calcula-

tion represents a convenience, and is not a computational restriction. This is treated in the next section. The second is the most obvious of a more general problem associated with ignoring nonlinearities. The specific influence of a variable surface stress forcing can be estimated to some extent through heuristic arguments. Its most impressive impact, as evident during the 1994 winter ANZFLUX experiment, is the extensive entrainment driven by turbulent mixing during the passage of frequent and intense storms [*McPhee et al.*, 1996]. These vent enormous amounts of TB_w without a corresponding reduction in SD_w due to ice growth. This particular response introduces nonlinearities in the form of discontinuities attributed to the transition from ice growth, or destabilization periods, to melting, or stabilization periods. Fortunately, for time-integrated quantities such as the bulk parameters, this type of nonlinearity effects a minimal seasonal impact and thus can be reasonably accounted for (though it may introduce other nonlinear influences or feedbacks, particularly through the covariation of external parameters and forcing that have not been anticipated or treated here).

The decoupling of TB_w and SD_w via storm-induced mixing events may, in the limit, result in the complete elimination of the thermocline and venting of TB_w, leaving SD_w essentially unchanged. SD_w is unchanged because the freshwater content of both the mixed layer and halocline is included in its calculation, thus the entrainment of the halocline into the mixed layer, while influencing the vertical distribution of the freshwater, does not influence the net amount of freshwater. Because TB_w and SD_w are intimately coupled under a smooth forcing, where salinization reduces SD_w while simultaneously venting TB_w, the time-dependent behavior of the variable forcing (storm) scenario will be quite different from that of the smooth forcing. However, when integrated to the limits of stability, both scenarios ultimately require the same amount of net *in situ* ice growth to eliminate SD_w.

Even though SD_w is not altered by storm events, the bulk stability, Σ, of the water column can be. The storms erode the pycnocline, mixing the TB_w enthalpy into the mixed layer. This changes the nature of TB_w venting from a negative feedback as described for the linear winter, to a direct venting, comparable to that in summer (which is independent of SD_s). Given a large enough mixing event, the vented TB_w may have the potential to melt more ice than present and/or significantly reduce the ice concentration. In either case, the venting of TB_w to the atmosphere through a reduced ice concentration is considerably more efficient than that expected during the smooth forcing scenario. Therefore, the storms may effectively reduce TB_w as an ice-growth-inhibitor equivalent. If the entire TB_w is vented in one storm, a limiting, albeit unlikely, scenario, its influence on the freshwater balance will be restricted to being less than or equal to the local ice thickness, h_i. That is, it cannot put more freshwater into the surface layer than it can melt (h_i).

In regions where the pycnocline stratification is weak enough to allow a significant or complete turbulent erosion of the thermocline during intense storms, the bulk stability may be reduced from $\Sigma = TB_w + SD_w$ to $\Sigma_e \approx h_i + SD_w$, the latter being the effective bulk stability. Throughout much of the seasonal ice region $h_i \sim 0.6$ m [*Wadhams et al.*, 1987; *Ackley et al.*, 1990; *Eicken and Lange*, 1989]. So, wherever TB_w is substantially larger than h_i, storms can introduce a substantial decrease in ocean stability.

For the other winter parameters, the decoupling of TB_w and SD_w alters the nature of the time-dependent behavior relative to the linear case, but should not significantly alter the overall seasonal interpretation of the parameter. The veracity of this statement is to a large part dependent upon the averaging used to compute the external parameters and their uncertainty. For example, the value used for ∇T when computing F_{DT} must represent a temporal mean accounting for differences preceding and following storms, and the variability about the mean must be incorporated into the uncertainties of the ultimate parameter estimate.

In summer, storms may initiate winter conditions before ice growth eliminates the seasonal halocline, thus venting TB_s but leaving a fresher winter mixed layer than otherwise expected from the steady forcing scenario. Therefore SD_s, as an estimate of fall ice growth, is an upper limit which conveys the potential for rapid ice growth contribution. However, because the fall ice growth is so rapid, the storms must occur within a relatively short window of time (during the fall growth, or just before it) in order to alter this particular estimate.

We are not sure of the degree or nature of additional nonlinearities that may be associated with storm events, or the variable surface stress forcing in general, so additional refinements may still be required. For example, there may be a strong covariance between storms, pycnocline doming (influencing mixed layer depth among other things), ice divergence and effective salinization distribution, K_z and lead area through increased surface divergence, driving nonlinearities or feedbacks that are not presently accounted for and that ultimately drive the net seasonal response from that expected for the

smoothly forced linear system. A potentially more important impact of such storm induced effects however, is their influence on the upper ocean structure that controls the external parameters (e.g., mixed layer depth and pycnocline thickness), and thus controls the linear bulk parameters directly. From this perspective, even the linear analysis presented here may account for a significant influence of persistent storm tracks.

3. METHODS

Data Base

Antarctic CTD station data collected between the Antarctic Peninsula and 20° E, during 28 cruises conducted over the last 25 years were used in this study. These data are readily available from the NOAA Ocean Data Center, the Alfred-Wegner-Institut für Polar- und Meeresforschung, the Nemo Oceanographic data server at Scripps Institution of Oceanography, and from *Heywood and King* [1996]; a complete listing (as well as a postscript version of this paper) is provided in the dgm home page at http://www.ldeo.columbia.edu:80/~dgm/ (or link through the Lamont-Doherty Physical Oceanography Web site: http://www.ldeo.columbia.edu).

Of the initial 2016 CTD station profiles available from the 28 cruises, 306 were rejected immediately because they resided outside of the polar gyre or were incomplete (large data gaps or missing variables). The remaining 1710 stations were then processed, as described below, and inspected at several stages to cull severely corrupted data or those whose shape deviated significantly from the ideal shapes of Figure 1, preventing identification of the integration limits. This hand culling eliminated another 287 stations leaving a total of 1423 stations used to construct the climatologies. The surviving 1423 hydrographic station locations used in the analysis are identified via small white dots in each of the parameter maps of the next section. The winter parameters are computed using all 1423 stations (as described previously), but only 715 stations are available for the summer calculations, thus these latter results are rather sparse and can only demonstrate the concepts and describe the broadest sense of the features.

Typical temperature and salinity profiles, are shown in Figure 1 superimposed on the ideal profiles to give an indication of how they look relative to the ideal shapes, though, as described below, it is important to realize that the parameter calculations are based on the true profile shapes, not the ideal shapes; the latter are derived strictly to facilitate the error analysis (which takes into account deviations of the true shape from the ideal ones), and to allow quick estimation of the parameters from profiles without performing a full integration.

Data Processing

Smoothing. Most of the T and S profiles were recorded at 1 db intervals. Those recorded at lower vertical resolution were interpolated to 1 m resolution so that the same vertical smoothing function could be applied to all profiles, though this diminished the effective level of noise reduction in the more coarsely sampled profiles. The data were smoothed with a 19-point vertical median filter. A rather extensive set of tests suggested that the bulk parameter estimates were extremely robust to the actual degree of smoothing and type of smoother applied. Consequently, the filter width used here was determined experimentally and found to provide the minimal filter necessary to qualitatively smooth the noise from the profiles while not overly destroying the critical features within it.

Parameter calculations. To avoid uncertainties associated with deviations of the true profiles from the ideal, the parameters are calculated by vertically integrating heat, salt and buoyancy through the upper water column, over the appropriate limits. In order to partition the different sources of heat and salt into their natural physical constituent components (e.g., differentiating the deep TB_w from the shallower TB_s), integration limits are defined at several critical features within the upper ocean profiles. The critical features are labeled in Figure 1. Most of these are identified based on their physical interpretation and thus uniquely identifiable during the integration itself. For example, the lower integration limit is typically the depth at which no additional salinization is required to drive overturn of the water column, z_{wc}. In other words, once the mixed layer deepens to this point by the elimination of the SD_w, cooling the mixed layer back toward the freezing point is sufficient to drive additional convection, so that deep overturn is essentially assured.

Similar arguments apply to all other points in the water column except for the interface between the winter mixed layer and permanent pycnocline, z_{wm}. This feature is the critical limit from which most summer integrations end and most winter ones begin. Identification of z_{wm} is done through use of a penalty function which seeks the maximum curvature of a normalized smoothed salinity profile, with the minimum deviation from the mixed layer salinity. That is, it rewards high curvature, but recognizes that some deeper feature within the

pycnocline such as a step, intrusion or other abrupt feature may actually possess the global curvature maximum. Thus, it penalizes for deviating from the mixed layer salinity, which proceeds quite rapidly with depth in the pycnocline. The normalized salinity profile, $S^*(z)$, is given by:

$$S^*(z) = S(z) - \frac{1}{z}\int_0^z S(z)dz \qquad (5)$$

This quantity is the salinity perturbation from the mixed layer salinity, given mixing to any depth z.

Once the integration limits are picked, the fundamental parameters can be computed according to the geometric relationships provided in (1) - (4), or via the full depth integration. The difference between these two estimates is a measure of how much the profiles deviate, nonsymmetrically, from the ideal profiles. This difference is relatively unimportant when full profiles are available, since the depth integrated values used here are accurate and easily calculated. However, the more simple geometric calculations are important for assessing the sensitivities of the parameters to changes in the external parameters (e.g., by computing the derivatives with respect to the external parameter of interest). They are also good for quick assessments of profiles, and ultimately for model-based computations where the deviation from ideal should be minimal in most cases and the depth integration too computationally-intensive to compute regularly.

While there is considerable variability across the gyre, typical values of the integration points, defined in Figure 1, are as follows: $z_{wm} = 117 \pm 46$ m, $z_{wc} = 205 \pm 94$ m, $z_{sm} = 22 \pm 22$ m, $z_{sc} = 57 \pm 41$ m. Source code for the depth-picks and integrations to produce the various parameters presented here can be obtained from the web site (dgm home page) listed previously.

Uncertainties

Several types of uncertainties are expected in the parameter values: (1) methodological error (random and bias), reflecting the ability of the penalty function to capture the desired physical characteristic, (2) analytical error, reflecting the precision with which the critical features in the profiles can actually be located, (3) temporal variability, (4) temporal bias, arising from the time of season when the profiles were acquired, and (5) sampling errors.

The methodological and analytical errors are dominated by the uncertainty in identifying the mixed layer-pycnocline interface depth, z_{wm}, which is difficult due to smearing by turbulent diffusion, though entrainment tends to drive the interface back toward the ideal profile shape in Figure 1. The other critical features (integration limits) are identified via physically unique criteria as previously described and are consistently identified within a smoothed profile to the resolution at which the profile is sampled; typically one or two meters for the data available here.

Methodological error (random error and bias). The methodological error reflects the ability of the penalty function to pick that z_{wm} which is representative of the physical characteristic sought; in this case, the boundary between the mixed layer and pycnocline. This error manifests itself in two stages. The first involves the variables used in the penalty function and its functional form. The second involves the ability of the optimal penalty function to identify the interface, given irregular profile shapes and smearing by diffusion. These are addressed by generating a set of control profiles with a known interface depth that have then been subjected to varying degrees of diffusive smoothing (applied as a cascading filter, and spanning a range comparable to that present in the data set). This testing involved a variety of penalty functions and variables (e.g., T, S and ρ profiles, and various hybrid combinations), which led to our ultimate choice of penalty function described above.

Further testing revealed that the diffusive smearing of the mixed layer-pycnocline interface introduces a bias in the pick, with a precision about the biased-pick of better than ±2 m (the methodological random error). The bias itself, ε, is as large as 10 m shallower than the true z_{wm}, though the typical bias appears to be 2-3 m. It also shows a functional dependence on the local curvature ($\partial^2 S/\partial z^2$) at z_{wm} and ∇S through the pycnocline (that is, the angle at which the pycnocline intersects the mixed layer). The steeper the pycnocline, the stronger the bias. The functional relationship of the bias to the curvature and halocline slope was determined by two-dimensional regression, of the form:

$$\varepsilon = a_1 + a_2 \log(\nabla S^{*2}) + a_3 \log\left(\left.\frac{\partial^2 S^*}{\partial z^2}\right|_{z_{wm}}\right) \qquad (6)$$

with $a_1 = -5.47$, $a_2 = 16.57$ and $a_3 = -10.26$. This correction captures ~54% of the bias variance.

Despite what appears to be a rather large bias in the actual location of z_{wm}, its influence is minor in the actual parameter values. This is because the integration in the vicinity of this interface (and shallower, in the direction of the bias) is over a nearly vertical (no-property change) slope, and thus, even though it covers ≤10 m

depth, its net contribution to the total property integral is trivial; for example, it introduces errors of ~3-4% in SD_w in the representative cruises for typical bias (2-3 m), and <11% error for the infrequent but worst case bias. Consequently, because of the weak influence and our mediocre success with (6), we did not apply the bias correction before processing the data.

Analytical error. The analytic error, i.e., the ability to precisely pick a unique z_{wm} depth, is related to the curvature and noise level in the profile at z_{wm} (ignoring the second component of the penalty function that simply prevents the picking of a feature with stronger curvature elsewhere). Conceptually, the stronger the curvature relative to the level of noise in the profile, the more uniquely a maximum can be identified. The weaker the curvature relative to the noise level, the larger the uncertainty in identifying the maximum. This error is estimated by $[\sigma_S/(\partial^2 S^*/\partial z^2)]^{1/2}$, where σ_S is the typical sample standard deviation in the S^* profiles (in the vicinity of the interface) from which the pick is being made.

For the data used here, the analytical error is typically quite small, ~0.65 m — comparable to the resolution of the data itself (based on analysis of two cruises thought to be representative of the entire data base). This states that the profiles are smooth enough to allow a clear determination of the point of maximum curvature, so this error can be safely ignored as the resolution itself subsumes it.

Temporal variability. While the above errors are generally small and manageable, the major source of uncertainty is associated with vertical migrations of the water column, possibly in response to surface forcing variations. These temporal migrations are difficult to separate from spatial variability, but can be estimated from the rather extensive buoy data archives [*Sellmann and Kottmeier*, 1996; *Kottmeier et al.*, 1997]. Examination of the longest duration temperature-depth sections along drift tracks suggest average changes in mixed layer and pycnocline thicknesses (h_{wm} and h_{wp}, respectively) of, $\sigma_{h_{wm}} \sim 15$ m, and $\sigma_{h_{wp}} \sim 12$ m, for the winter months. The excursions appear to be slightly smaller for summer months. For both seasons, the intra-seasonal covariance between h_{wm} and h_{wp}, $\mathrm{cov}[h_{wm},h_{wp}] < 5\%$.

The influence of $\sigma_{h_{wm}}$ and $\sigma_{h_{wp}}$ on errors in SD_w and TB_w is estimated via the expectance operator. Specifically, since TB_w and SD_w are both linear in h_{wm} and h_{wp}, the variance of TB_w scales linearly with $\sigma^2_{h_{wp}}$, the scaling factor given by $[(T_{wp}-T_f)\rho_w c_w/2\rho_i L_i]^2$; the variance of SD_w scales linearly with the sum of $\sigma^2_{h_{wm}}$, $\sigma^2_{h_{wp}}/4$ and $\mathrm{cov}[h_{wm},h_{wp}]$ (<5%, so neglected here), the scaling factor given by $[(S_{wp}-S_{wm})/\sigma]^2$. So, $\sigma_{h_{wp}} \sim 12$ m and $\sigma_{h_{wm}} \sim 15$ m contribute to temporal uncertainties in TB_w and SD_w of $\sigma^t_{TB_w} \sim 0.05$ m and $\sigma^t_{SD_w} \sim 0.02$ m, respectively, for typical T and S differences across the pycnocline near the gyre center.

For climatologies, in the densely sampled regions, we typically average 3 to 5 data points, reducing $\sigma^t_{TB_w}$ and $\sigma^t_{SD_w}$ by half (though the reduction is not completely realized since some spatial variability is introduced during climatological averaging within spatial bins). For parameters involving differences or ratios, this error is again inflated by the operation, which approximately doubles it back to the original, unaveraged size. In either case, the temporal variations introduce errors of 5-10% at most of the station locations ($\sigma^t_{SD_w}/SD_w$ is constant for any particular $h_{wm}\pm\sigma_{h_{wm}}$ and $h_{wp}\pm\sigma_{h_{wp}}$, thus $\sigma^t_{SD_w}$ can be given as a percentage of SD_w; likewise for TB_w and $\sigma^t_{TB_w}$). More importantly, the temporal errors are more than an order of magnitude smaller than most of the spatial variability displayed in the parameter maps below, so they preserve a very good spatial signal-to-noise ratio of ~20 db.

The temporal variability subsumes the smaller analytical and methodological uncertainties discussed above in all but the limiting cases.

Temporal bias. This bias arises because the parameters, which represent seasonal limits, are determined from observational profiles that were not necessarily acquired at the start of the season. Therefore, some of the seasonal evolution has already occurred, but the parameters have not been corrected for this. SD_w for example, represents the amount of freshwater in the surface layer that must be removed by ice growth in order to overturn the water column. If the profile from which this quantity is calculated was taken in mid-winter, some fraction of SD_w will have already been eliminated by ice growth that does not appear in the calculation. Therefore, there is a bias associated with each parameter estimate that is proportional to the length of time that has elapsed since the start of the relevant season.

This temporal bias influences the interpretation of the data in all situations, not just those involving the bulk parameters presented here, so an estimate of its impact is necessitated for all analyses. In order to properly correct for this bias we need estimates of winter ice growth and entrainment rates, and the time of onset of the various seasons from either the data or models. At present, this information is nominal for both the data and models. Comparing ice thickness changes through time from data suggests that the ice undergoes a minimal growth of $\sim 1.6\times10^{-3}$ m day^{-1} [*Wadhams et al.*,

1987] in winter, while simple model estimates suggest ~1.3×10^{-3} m day^{-1} [*Martinson*, 1990] (these are ~25 and 20 cm per 5 months of winter, respectively). For every month that passes following the onset of winter conditions, SD_w is thus decreased by ~0.04-0.05 m. For entrainment rates, the modeling [*Martinson*, 1990] suggests mixed layer deepening of 0.03-0.12 m day^{-1}, the smaller values in regions where TB_w is smallest, so the bias approximately scales with TB_w. TB_w varies proportionally to mixed layer deepening at about 2% of the change in depth; that is, for every month that passes following the onset of winter, the above estimates suggest that TB_w decreases by ~0.02-0.07 m. Therefore, data acquired in late winter may introduce a bias as large as 30% or so, while data from early winter introduces a bias of <5%.

At present, we do not correct for this bias given the questionable quality of the model and limited data estimates. Consequently, the values may under-estimate some of the quantities they purport to represent. Data acquired exceptionally late in the seasons were not included in the analysis to minimize their particularly large impact on the bias. The remaining data from different times within a season should average out the bias toward mid-season values, typically around 10-30%. Furthermore, the bias is expected to be spatially homogeneous and thus should not significantly reduce the spatial signal-to-noise ratio in the parameter maps below.

Sampling Error

Sampling errors are assumed to be responsible for "bad" profiles — those that display grossly uncharacteristic shapes (relative to surrounding stations) or contain exceptional data values. The majority of these profiles were identified and eliminated prior to processing as described previously. However, a second attempt at eliminating bad profiles was made upon completion of the processing by examining those profiles responsible for introducing any exceptional features in the parameter spatial distributions (e.g., local minima or maxima). Only one isolated feature from the parameter maps was eliminated as a result of this particular quality control measure.

4. RESULTS

Climatology Maps

The various parameters discussed above have been computed for each station using the real profiles. Using the GMT gridding program [*Wessel and Smith*, 1991; *Smith and Wessell*, 1990], station values for individual cruises are then interpolated spatially onto a tight, 0.25° (latitude) x 0.5° (longitude) grid using a taut spline that minimizes overshoot across abrupt gradients and is constrained to minimize overshoot at the boundaries, which reduces the already small interpolation error at the edge of grid cells. Parameter values within this grid are then averaged through time onto a broader 0.5° (latitude) x 1.0° (longitude) grid to produce a climatological (time-averaged) spatial distribution for each. The climatology grid size approximates the typical spatial decorrelation lengths within the eastern region, where spatial variability is highest, so the bin size should be a reasonable estimate throughout the remainder of the gyre region.

The spatial averaging also accounts for the influence of lateral fluxes in the vertically-integrated bulk parameter values, thus extending the spatial range of the parameter maps. North of the polar front, however, these fluxes begin to dominate and the vertical distribution of ocean properties is such that the underlying assumptions of the analysis become questionable and should be ignored. The position of the polar front, according to *Orsi et al.* [1995] is indicated in Figure 2 and on each of the parameter maps. The parameter values are computed for regions north of this front, but the values frequently lie well outside the standard range and are not included on the color scale of the maps; instead they appear as white color ("off scale"). As seen in the maps, this white region often appears just north of the polar front, and thus the parameters themselves seem to nicely delimit the natural boundary of the polar gyre.

Also, in the vicinity of the perennial ice in the western Weddell Sea, indicated in Figure 2 by the February ice extent, the parameter interpretations become equivocal since the seasonal conditions assumed elsewhere in the gyre are not applicable in the perennial region. Therefore, while some of the parameters still have a physical interpretation of interest, they may not be consistent with the broader interpretation presented for the rest of the gyre. The discussion here is thus limited to the broad gyre-scale implications and basic concepts. More detailed discussion regarding particular parameters or their spatial and temporal variability will be given elsewhere.

In order to relate the spatial distributions to the gross features of the Weddell gyre region, and delimit the regions discussed above, Figure 2 presents the bottom topography, position of summer and winter ice extents, and polar front.

Winter thermal barrier. The winter thermal barrier is presented in Plate 1. The TB_w is seen to clearly re-

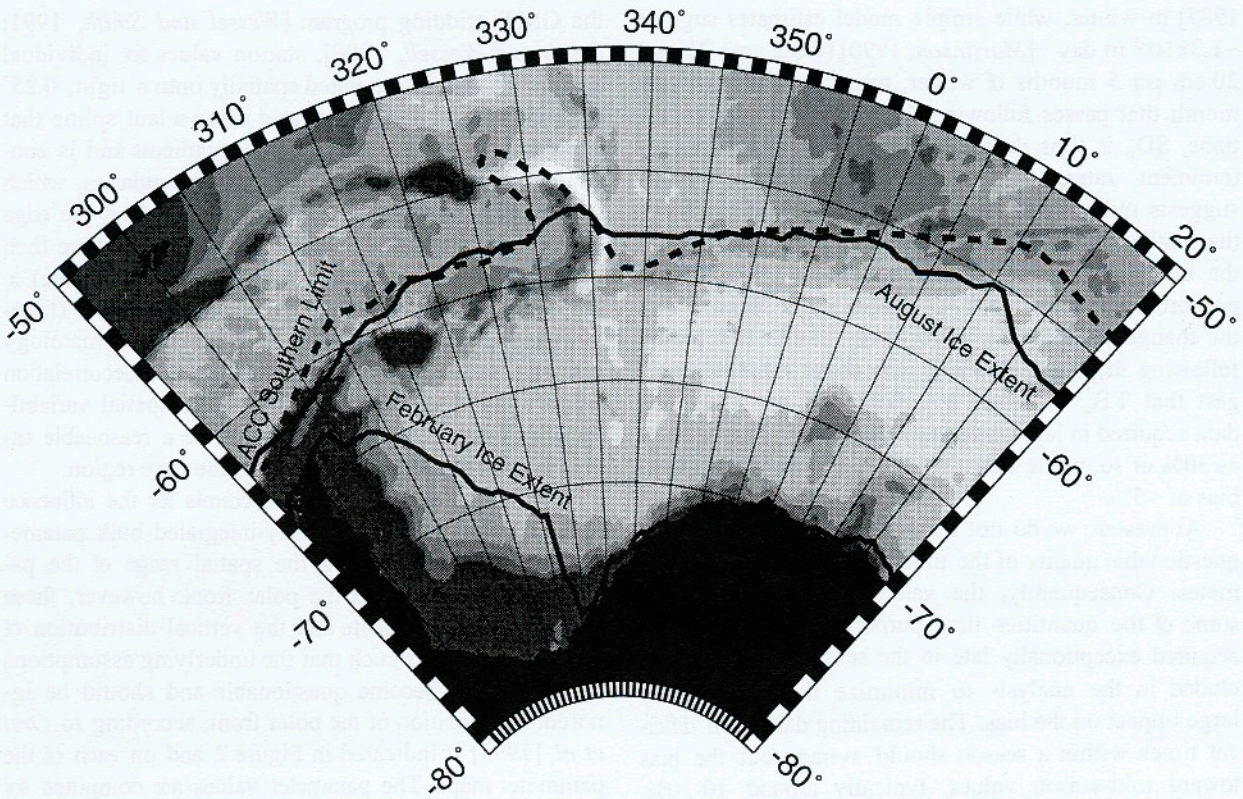

Figure 2: General physical setting and characteristics of the Weddell gyre region. Bottom topography is shaded at 1000 m intervals; the winter (August) and summer (February) ice extents are indicated by solid lines (the latter represents the extent of the perennial ice cover in the region); the approximate location of the southern limit of the Antarctic Circumpolar Current, as defined by *Orsi et al.* [1995] gives the approximate location of the northern limit of the polar gyre.

flect the gyre geometry, with increasing TB_w near the gyre margins where reduced upwelling allows a broader thermocline that contains more stored enthalpy. TB_w depends predominantly on the thickness of the pycnocline (Plate 2) with ~48% of its variance attributed to this specific water column characteristic. As seen in the gyre's zonally elongated core (~66° S), stronger upwelling leads to a thinner thermocline that stores only enough heat to melt ~0.5 m of ice (i.e., a relatively weak thermal buffer), whereas TB_w is an order of magnitude larger at the margins. Note that at the northern margins, even if lateral (ageostrophic) fluxes begin to play a dominant role in the property balance, additional spatial averaging would accommodate these fluxes. As clearly evident from the figure, such additional averaging, while smearing the zonal TB_w gradient somewhat, will not eliminate this overall rapid increase in its value at the northern margins of the polar gyre.

Winter salt deficit. The total amount of salt required to eliminate the winter surface freshwater content, SD_w^T, is presented in Plate 3. It shows a distribution somewhat similar to TB_w, i.e., reflecting the gyre geometry, though the relationship is not quite as clear. As seen, the surface freshwater content throughout the vast majority of the central Weddell gyre is less than 0.5 m of equivalent ice growth. Toward the northern extreme of the gyre, particularly in the east where the Antarctic Circumpolar Deep Waters enter the Weddell gyre, SD_w^T increases by a factor of two or three. This may reflect the northward and eastward drift of the sea ice and thus a convergence of ice melt in those regions.

An estimate of that portion of the salt deficit which is eliminated by non-ice related sources of salt, SE, is shown in Plate 4. The entrainment-driven salt flux is relatively small given the predominant role of salinity on density, so $\Theta_{DS} >> \Theta_{ES}$ and $SE \approx \Theta_{DS}$ in all but a

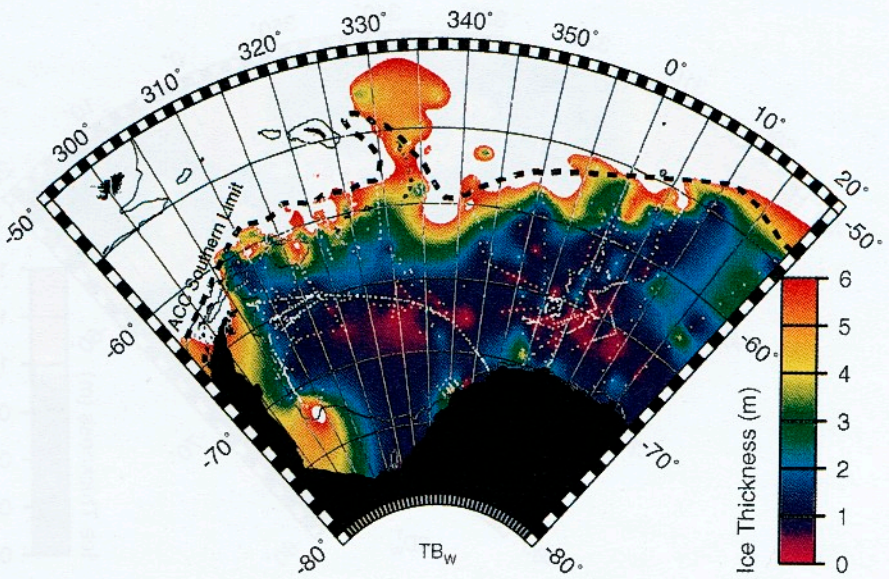

Plate 1: Winter Thermal Barrier (TB_w) in units of equivalent units of ice thickness (i.e., how much ice can be melted by enthalpy content of the thermocline). White areas exceed the standard range of the parameter within the polar gyre (they are "off scale"); 1000 m depth contour is given to indicate approximate location of shelf-slope break; dashed line shows approximate northern limit of polar gyre.

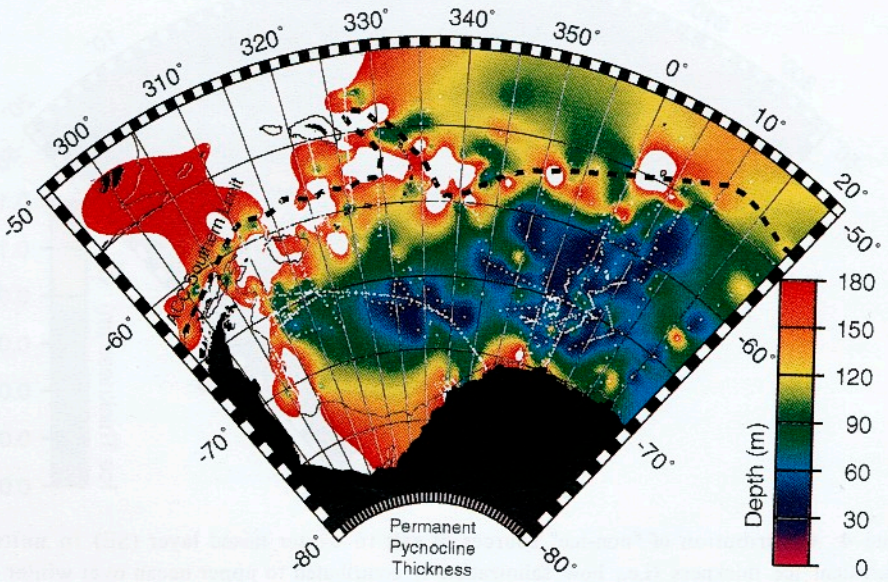

Plate 2: Permanent pycnocline thickness. Contours and white areas as in Plate 1.

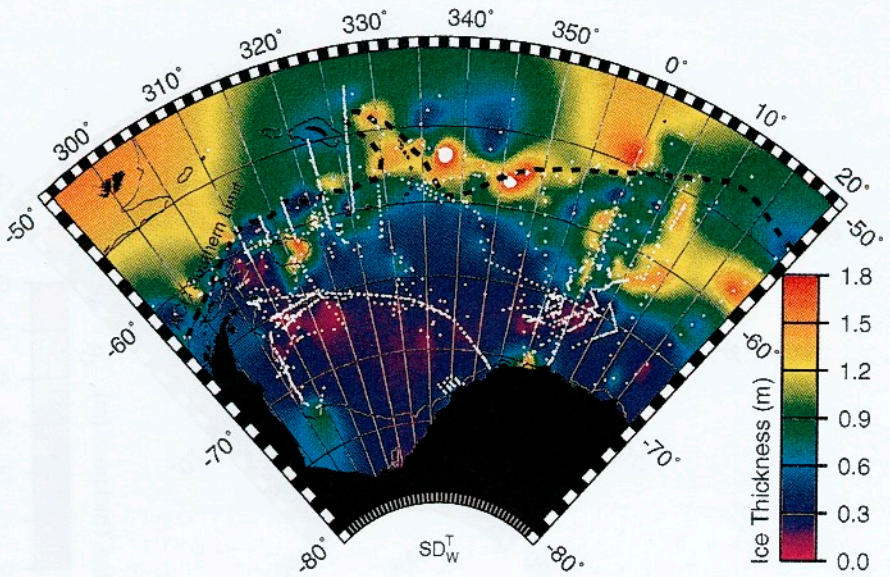

Plate 3: Total Winter Salt Deficit (SD_w^T), given in units of equivalent ice thickness (i.e., how much ice must grow to inject enough salt into the surface ocean to eliminate stabilizing fresh-water layer). Contours and white areas as in Plate 1.

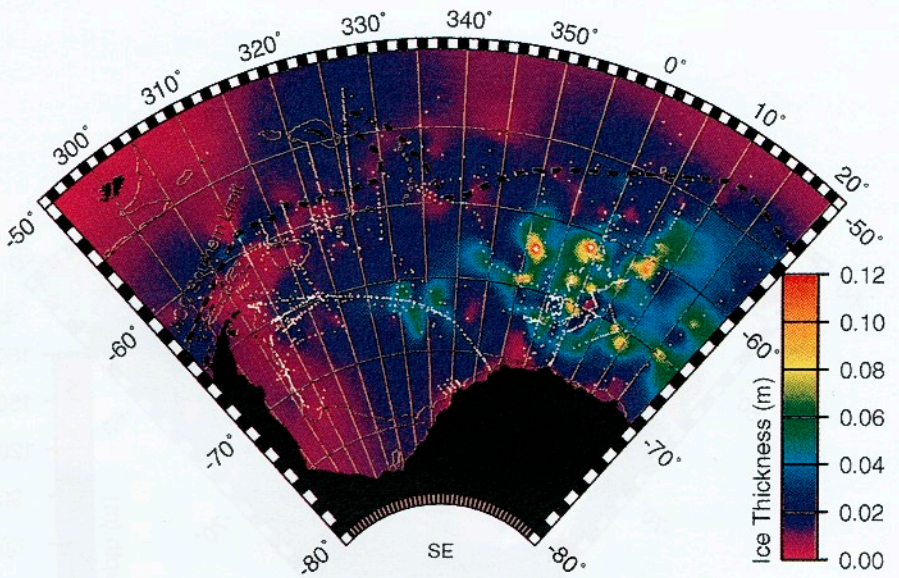

Plate 4: Contribution of "non-ice" sources of salt to winter mixed layer (SE) in units of equivalent ice thickness (i.e., how salinization is contributed to upper ocean over winter due to sources of salt other than ice growth). This is predominantly an indication of diffusion across the pycnocline. Contours and white areas as in Plate 1.

few locations where the halocline is exceptionally weak due to abnormally large thickness. Therefore, Plate 4 is an approximation of the diffusive salt flux. Since this diffusion is proportional to the pycnocline thickness, the largest values coincide with the thinnest pycnocline, as shown in Plate 2.

Applying the SE correction to the total salt deficit, SD_w^T, gives the corrected winter salt deficit, SD_w (Plate 5). Because SE is small, typically <0.05 m, its influence on the pattern of SD_w^T is minimal so SD_w shows a similar pattern. This is not true near Maud Rise (65° S, 0° E) however, where SE represents a relatively large contribution to a relatively small SD_w^T resulting in the near elimination of SD_w^T. In other words, in that area there is a minimal stabilizing freshwater cap since the freshwater present can be almost eliminated by oceanic processes alone in the absence of an ice growth salinization contribution. Bulk stability here is most likely maintained by the stabilizing influence of the strong diffusive heat flux (shown below) and/or the potential influence of lateral processes in this rather spatially heterogeneous region. Given the latter, the bulk parameters still provide the desired spatially-averaged limitations and constraints when integrated over a slightly broader spatial area so that the full upper water column budget is properly accounted for.

SD_w indicates the maximum net thickness of *in situ* ice growth that can be realized in winter since any more ice growth rejects enough salt to overturn the water column. The gross ice thickness (more accurately, the heat loss in units of equivalent ice thickness) is equal to $SD_w + TB_w$, but venting of TB_w melts (or inhibits from growing) an amount equivalent to TB_w whose meltwater must then be overcome by growth of an amount equivalent to TB_w again. Thus, SD_w is ultimately the maximum *net* amount of winter *in situ* ice growth. The maximum amount of annual ice growth is the fall plus winter ice growth, or $SD_s + SD_w$.

Throughout much of the central gyre region the amount of ice growth required to eliminate the freshwater storage in the winter mixed layer is fairly small, typically ≤0.30 m (as previously stated, this is in addition to the fall ice growth, SD_s).

Bulk stability. The bulk stability, Σ, is shown in Plate 6. Consistent with the comments above, the least stable portion of the gyre lies along the zonal core where approximately 1 m or less of total winter ice growth, or its heat loss equivalent, overturns the water column. The minimum value occurs near the Greenwich Meridian and is equivalent to ~0.2 m. However, at this location, near Maud Rise, the lateral processes may be significant contributors to the OAI interaction and compromise the vertical bulk stability value suggested here [*Gordon and Huber*, 1984; *Bersch et al.*, 1992].

Near the gyre rim the bulk stability is approximately 5-9 m of *in situ* ice growth. There, the ability to resist overturn is formidable despite the weak pycnocline, relative to mid- and low-latitude profiles, and relative to the typical magnitude of the forcing, which is sufficient to grow approximately 3 m of ice in the absence of the ocean heat flux [*Martinson*, 1993].

The potential influence of storms on the bulk stability, that is, $\Sigma_e \approx h_i + SD_w$, is grossly approximated by assuming $h_i \sim 0.6$ m as discussed previously. This is a simple scaling of SD_w and is presented by the lower-left color bar in Plate 5. As seen, while the pattern is fairly similar to that of bulk stability (Plate 6), the Σ_e values are considerably reduced in those regions where TB_w is large (along the gyre margins). Storm-induced bulk stability reduction is less in the central gyre region where TB_w contributed less to the bulk stability initially.

While the absolute reduction in Σ is relatively small throughout the central gyre relative to the reduction at the gyre margins, bulk stability is still reduced by ~40% by storms (as seen below, TB_w represents a considerable fraction of bulk stability even in its weakest locations). This parameter needs to be supplemented by one estimating the amount of ventilation expected per typical storm, and one estimating the magnitude of storm required to completely ventilate TB_w, in order to determine which areas are most susceptible to realizing the full bulk stability reduction by storms.

Plate 7 shows that fraction of bulk stability that is attributable to TB_w, $\gamma_{TB} = TB_w/\Sigma$. This clearly reveals that bulk stability throughout most of the area is due to TB_w, that is, to the deep ocean heat, not the surface freshwater layer. In fact, TB_w accounts for 70-90% of the bulk stability throughout most of the region. Its influence is weakest near the Greenwich Meridian, where it still accounts for almost 50% of the bulk stability, and in a few regions where it gets as low as 30% where the thermocline is exceedingly sharp so its enthalpy content is quite small.

The effectiveness of TB_w in maintaining bulk stability is given by the ice melt to growth ratio, $\gamma_\Theta = TB_w/SD_w$ (Plate 8). As seen, the gyre is dominated by values of this ratio greater than 1. In these regions TB_w is sufficient to significantly dampen the winter ice growth to an effective growth rate of $(\gamma_\Theta+1)^{-1}$. Thus where the values are large, a significant amount of time

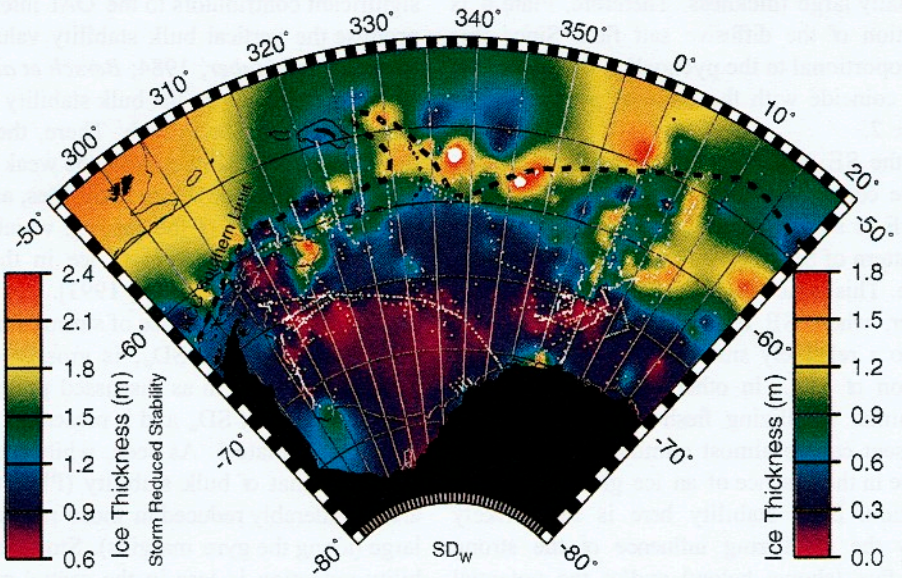

Plate 5: Winter Salt Deficit (SD_w), given in units of equivalent ice thickness (i.e., how much ice must grow to inject enough salt into the surface ocean to eliminate stabilizing freshwater layer after allowing for salt contributions by SE in Plate 4). Color scale on left indicates stability (see Plate 6) after accounting for potential influence of storms. Contours and white areas as in Plate 1.

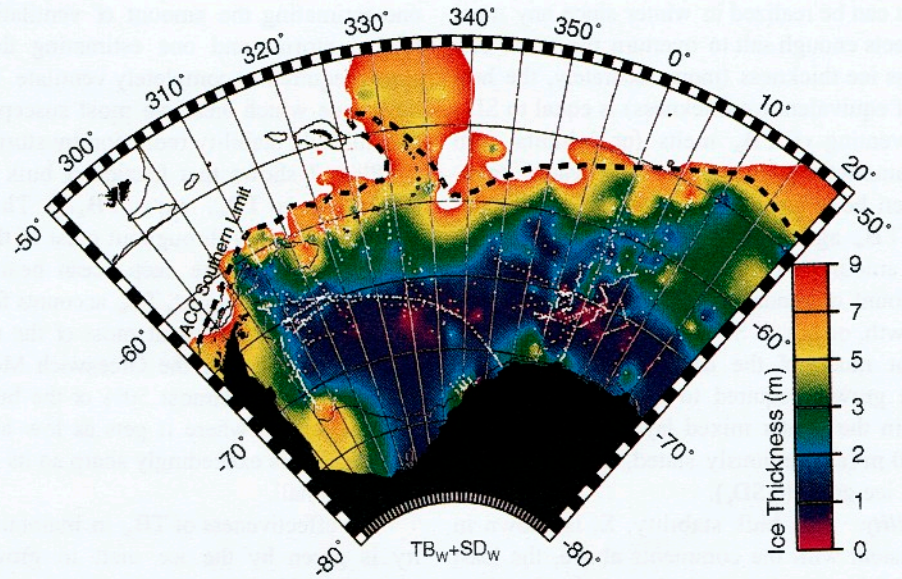

Plate 6: Stability (TB_w+SD_w), given in units of equivalent ice thickness (i.e., how much ice must grow to inject enough salt into the surface ocean to overcome both stabilizing freshwater layer and thermocline heat content, destabilizing water column, driving deep ocean convection and eliminating ice cover). Contours and white areas as in Plate 1.

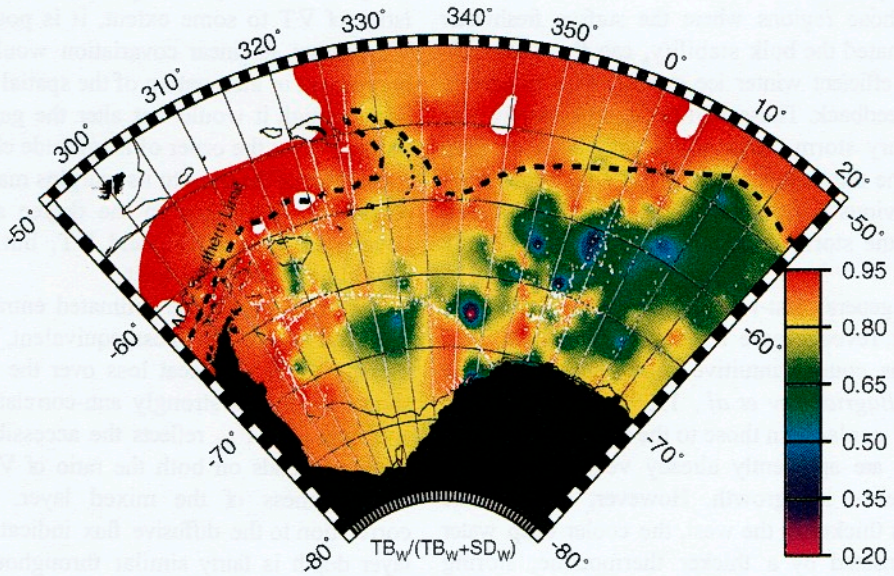

Plate 7: Winter Thermal Barrier fraction of Stability (TB_w/Σ). Indicates fraction of stability attributed to heat content of thermocline as opposed to freshwater content of surface layer (the latter related to ice growth/melt patterns). Contours and white areas as in Plate 1.

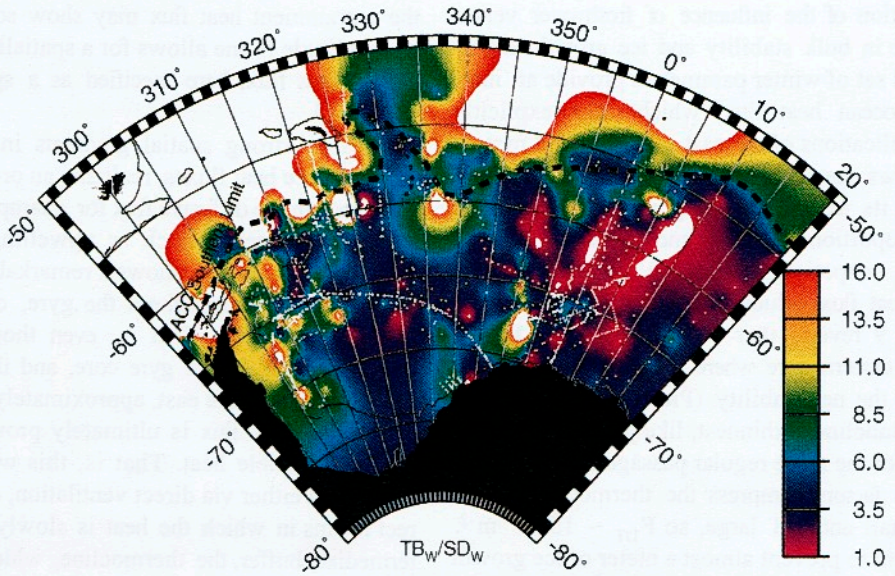

Plate 8: Ice Melt to Growth Ratio (TB_w/SD_w). Indicates how many units of ice are melted (by venting of ocean heat driven by ice growth salinization) for every unit of ice grown. Contours and white areas as in Plate 1, though in this figure, white areas also indicate regions in the parameter value less than the minimum value presented on the color bar.

will be spent under melt conditions with a minimal amount of ice growth.

Only in those regions where the surface freshwater content dominated the bulk stability, can the water column support efficient winter ice growth with respect to the negative feedback. These regions approximately parallel the primary storm tracks which may serve to keep the thermocline thin while venting the TB_w more effectively, as previously discussed. This may be a strong indication of the storm influence on the potential bulk stability.

Also, the general east-west trend, with smaller values in the east, reveals more feedback in the west. That initially seems counter-intuitive since the west is the cold regime [*Bagriantsev et al.*, 1989] where the deep waters are ~1° cooler than those to the east, and thus the deeper waters are apparently already vented, implying less resistance to ice growth. However, because the thermocline is thicker to the west, the cooler deep water is overcompensated by a thicker thermocline, storing more warm water closer to the surface and making it more accessible through a weaker stratification. In other words, the ocean can vent more heat per unit of ice grown, so the destabilization is more effective in tapping this stored enthalpy, even though the deeper water is cooler in an absolute sense.

Ocean heat flux. The parameters discussed so far give an indication of the influence of freshwater versus thermal storage in bulk stability and ice growth limitations. The final set of winter parameters provide an indication of the ocean heat flux, which more explicitly reveals the implications of the east-west increase in γ_Θ.

Plate 9 shows the winter-average eddy diffusive heat flux, F_{DT}, and its ice thickness equivalent, Θ_{DT}. Since this flux is proportional to ∇T and choice of K_z, the relative values, or spatial patterns, are more robust than the absolute heat flux values provided. From that perspective, Plate 9 reveals that the diffusive heat flux is highest in the eastern gyre where TB_w contributes relatively little to the net stability (Plate 7). This area is where the thermocline is thinnest, likely due to stronger upwelling and/or the more regular passage of intense polar lows. Both factors compress the thermocline which keeps TB_w small and ∇T large, so $F_{DT} \sim 15$ W m^{-2}. This is sufficient to prevent almost a meter of ice growth over the course of a 5-month winter growth season. Near the gyre margins, the thicker thermocline dominates, resulting in an order of magnitude reduction in diffusion.

Some fraction of the amplitude of the spatial pattern in F_{DT} may reflect the use of a spatially invariant K_z in its computation. Since surface stress influences the value of K_z and drives upwelling, which controls the characteristics of ∇T to some extent, it is possible that K_z and ∇T covary. A linear covariation would lead to an enhancement or attenuation of the spatial amplitude shown here, though it would not alter the general shape of the pattern. Thus the order of magnitude change in F_{DT} from the center of the gyre to its margins may in fact be larger or smaller depending on the degree and nature of any covariation between K_z and ∇T, but the pattern itself should be relatively robust.

Plate 10 shows the estimated entrainment heat flux, F_{ET}, and its ice thickness equivalent, Θ_{ET} assuming an average 35 W m^{-2} heat loss over the gyre. The pattern shown for F_{ET} is strongly anti-correlated with the diffusive heat flux. F_{ET} reflects the accessibility of the TB_w, which depends on both the ratio of $\nabla T/\nabla S$, as well as the thickness of the mixed layer. The close anti-correlation to the diffusive flux indicates that the mixed layer depth is fairly similar throughout the region and the dominant control on $\nabla T/\nabla S$ is the thickness of the pycnocline as described above.

The entrainment heat flux varies over the gyre by almost a factor of five, and it contributes enough heat to melt or inhibit from growing 0.4 to 1.7 m of ice (smaller values in the east and larger values in the west). Analogous to the situation with the diffusive heat flux, the entrainment heat flux may show some alteration of its amplitude if one allows for a spatially varying air-sea surface heat flux, here specified as a spatially invariant 35 W m^{-2}.

Despite strong spatial gradients in the entrainment and diffusive heat fluxes, realizing an order of magnitude difference in the diffusive flux for example, and reflecting gyre-scale processes such as upwelling, the total heat flux, $F_T = F_{DT} + F_{ET}$, shows a remarkably uniform value (± 30% change) throughout the gyre, of between 25-35 W m^{-2} (Plate 11). That is, even though the diffusive flux dominates in the gyre core, and the deep water is much warmer to the east, approximately 75% of a 35 W m^{-2} air-sea heat flux is ultimately provided in the form of ocean sensible heat. That is, this winter-average flux is realized either via direct ventilation, or via more indirect means in which the heat is slowly stored in an intermediate buffer, the thermocline, which is more easily eroded via surface-induced mixing, either by storms or free convection. If ∇T and K_z covary, it is possible that some spatial inhomogeneity may emerge in the total heat flux value, with the emerging pattern more similar to the diffusive heat flux spatial pattern.

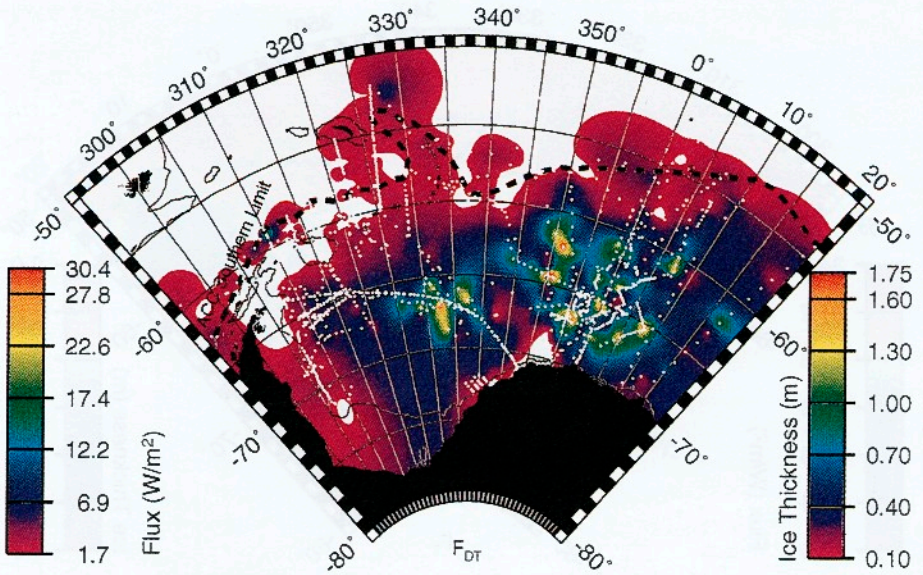

Plate 9: Average winter diffusive heat flux in units of W m^{-2} and in units of ice melt over the course of a 5 month winter. This value is proportional to the thermal gradient through the pycnocline, so the spatial pattern is more robust than the absolute numbers. Contours and white areas as in Plate 8.

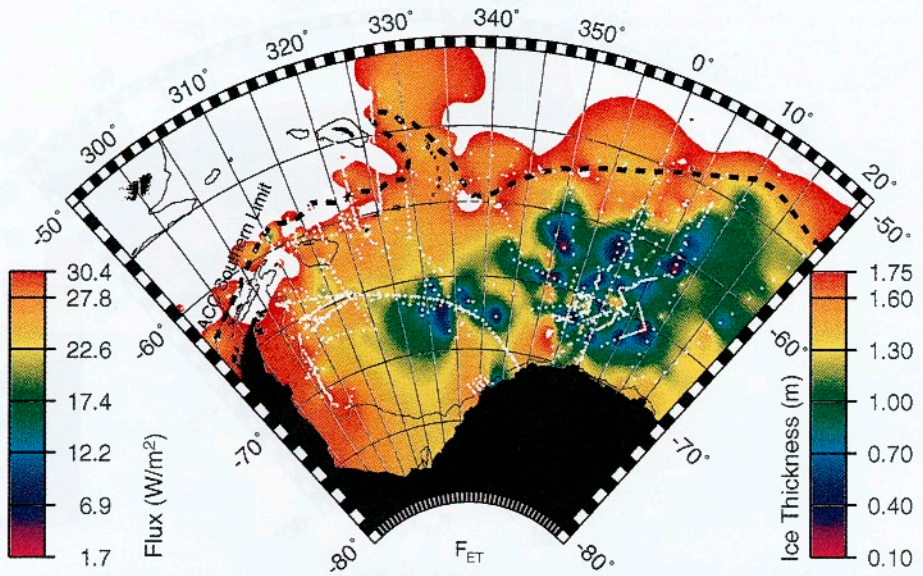

Plate 10: Average winter entrainment heat flux (units as for Plate 9). Estimate of ocean heat flux driven by entrainment in response to salinization during ice growth assuming a 35 W m^{-2} air-sea heat flux. As with diffusive heat flux, spatial patterns are likely to be more robust than absolute values. Contours and white areas as in Plate 1.

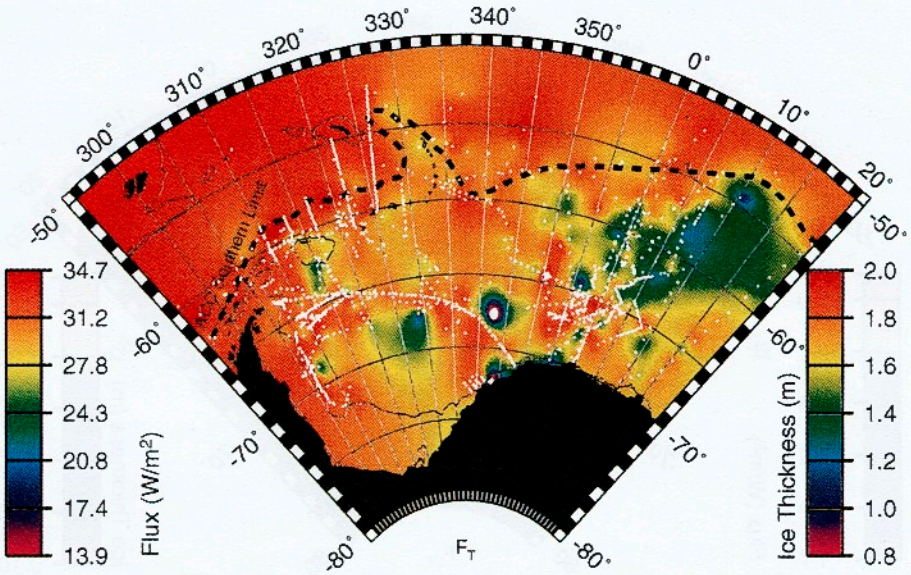

Plate 11: Total average winter ocean heat flux (units as for Plate 9). Sum of diffusive and entrainment heat fluxes. Note significant reduction in spatial variability relative to that of the two component fluxes (Plates 10 and 11). Contours and white areas as in Plate 8.

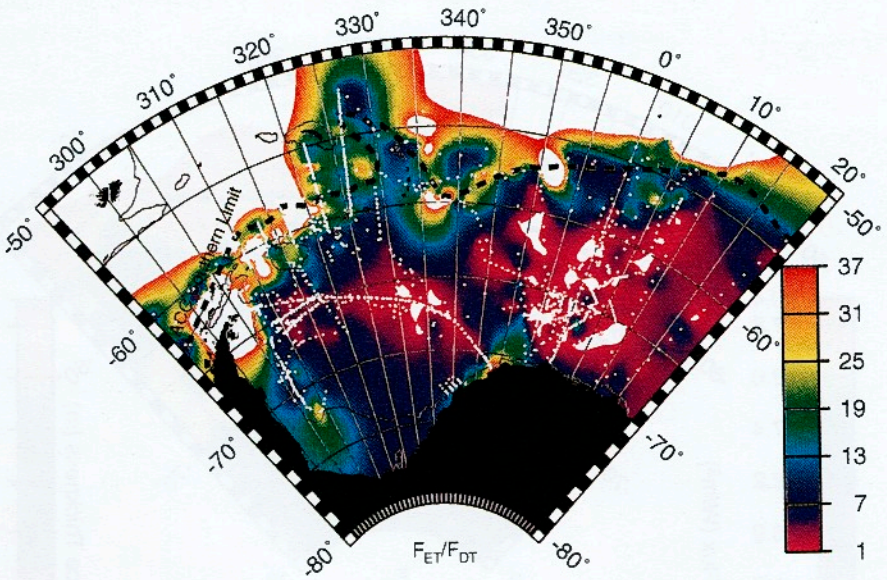

Plate 12: Ratio of average winter entrainment heat flux to average winter diffusive heat flux (units as for Plate 9). Indicates the mechanism by which heat is vented to surface. Where entrainment heat flux dominates (ratio > 1), the heat flux is predominantly driven by negative feedback in which ice growth drives entrainment and associated heat flux by salinization. Contours and white areas as in Plate 8.

Finally, Plate 12 shows the spatial patterns of the ratio between the entrainment and diffusive heat fluxes, $\gamma_T = \Theta_{ET}/\Theta_{DT}$. As seen, the entrainment heat flux is considerably larger than the diffusive heat flux in all but the core regions. Therefore, the storage of heat within the thermocline is a significantly more efficient way of venting heat from the system than simple diffusion which vents the deep water directly, but apparently far less efficiently.

The pattern here reinforces the concept that, where the pycnocline is relatively thick and the diffusive heat flux weak, ocean heat is predominantly supplied by an easily eroded pycnocline (whose enthalpy is replenished later via diffusion). In areas where upwelling brings the deep waters close to the surface (or storms bring the surface waters closer to the deep waters), exposing the deep water almost directly to the atmospheric interaction, the thermocline is stronger, and more resistant to erosion and heat release via entrainment, but it provides a considerably higher diffusive flux to accomplish a similar magnitude venting. Furthermore, where the diffusive flux is larger, ice growth is reduced so the entrainment heat flux is further inhibited by weaker salinization-induced destabilization.

Summer salt deficit. Plate 13 shows the summer salt deficit, SD_S, which varies from 0.2 - 1 m of ice. In the west, and north, the signal is predominately one of ice/snow melt, not growth because of the perennial ice cover. Also, given the relatively sparse summer data set, the values contain considerable uncertainty since we do not have enough samples to adequately average and make all of the necessary corrections, particularly removal of the temporal bias. However, the map does show a general reduction in SD_s from west to east, reflecting a thinner fall ice growth cover to the east. That is, the ice cover will be thinner in the east at the time when the winter conditions set in and the negative feedback mechanism becomes active, limiting further winter ice growth.

Critical interannual ice growth perturbation. Plate 14 shows the size of the perturbation in annual ice thickness required to destabilize the water column, $\Gamma_{ms} = 1/\gamma_{ms} = (SD_s + \Sigma_e)/SD_s$ (the relationship breaks down for reasons already discussed in the perennial ice fields to the west as indicated in Figure 2). In the eastern Weddell region, a couple of locations achieve ratios as low as 1.8. This indicates that the ice growth would have to exceed the annual climatological average by 80% in order to overturn the system. Unfortunately, the sparse summer coverage and temporal statistics are insufficient to provide decent spatial coverage, and to evaluate the likelihood of obtaining a perturbation of this magnitude during any one particular year. Once we obtain enough data to determine interannual ice thickness variance, we can estimate the likelihood of destabilization for any particular location. At present, the data can only demonstrate the concept and provide an indication of the approximate size of critical perturbations required in a few isolated locations.

Temporal Variability

The temporal variability in the various parameter values provides the variance, time-scales of variability and longer-term trends. These reveal tendencies for change, the magnitude of variability (allowing estimates of the likelihood of exceeding critical stability values as discussed above) and climate drift. Unfortunately, the current data base does not allow meaningful interannual comparisons since there is inadequate multi-year sampling with close enough spatial proximity, as dictated by local decorrelation lengths, to differentiate spatial from temporal variability.

For example, the area around Maud Rise has been sampled a number of times over the last couple of decades, but the actual overlap of stations within the local decorrelation lengths is quite small. Plate 15 shows bulk stability, Σ, for seven different years in this locale: 1977, 1981, 1984, 1986, 1989, 1992 and 1994. The parameters are interpolated between stations spanning gaps as large as 3° longitude, which is approximately three times the spatial decorrelation length. This large spread is necessary to convey some sense of the parameter distribution for comparison of one year to the next.

Focusing on the Greenwich Meridian at 65° S provides some sense of an increase in bulk stability in 1977 (immediately following restabilization of the area after termination of the Weddell polynya, *Zwally and Gloersen*, 1977). The values increase from ~0.7 m to ~2 m in 1984-1992, then decrease to ~0.5 m in 1994. Presently, it is difficult to distinguish whether this reflects a systematic change in bulk stability of the region, or minor spatial shifts in the presence of the extremely high local lateral gradients.

5. DISCUSSION AND CONCLUSIONS

The bulk parameters presented here are designed to encapsulate the physical essence of much of the ocean-ice interaction within the Antarctic polar oceans. In particu-

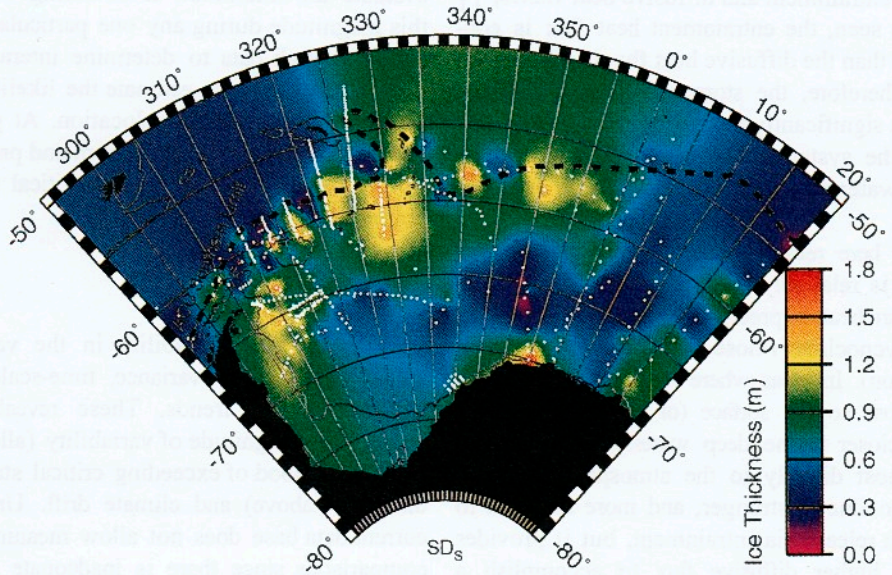

Plate 13: Summer Salt Deficit (SD_s). Similar to Plate 3, but for summer surface layer. Indicates amount of freshwater contained in summer surface layer, predominantly an indication of ice meltwater from previous winter, and an indication of how much ice will grow rapidly in fall before winter conditions are achieved and winter heat fluxes reduce ice growth rate. Contours and white areas as in Plate 1.

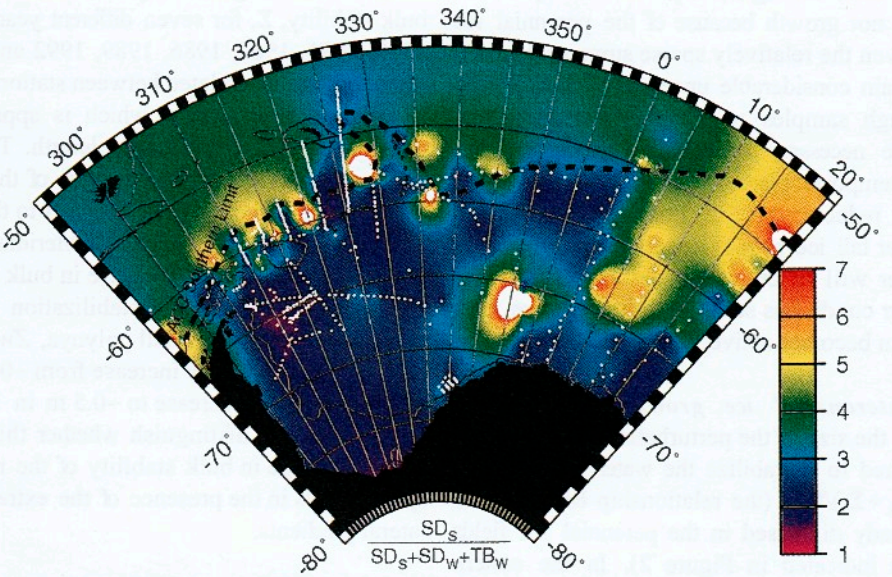

Plate 14: Critical Ice Growth Perturbation. This gives the amount of ice growth that is cycled each year through ice growth relative to the total amount of ice growth required to destabilize the water column. The fraction indicates how much of an interannual perturbation in annual average ice growth is required to destabilize the water column. Interpretation does not hold for the perennial ice regions in the western Weddell Sea. Contours and white areas as in Plate 1.

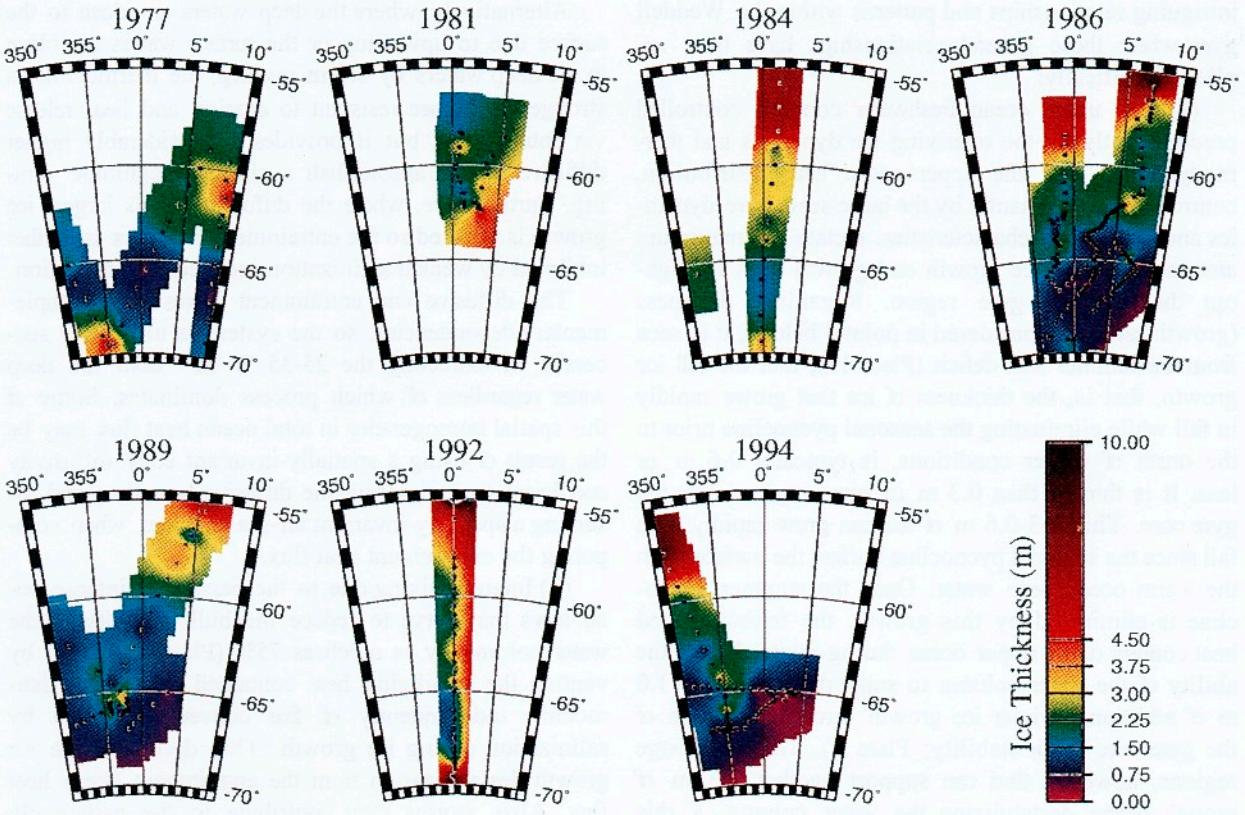

Plate 15: Stability (as in Plate 6) for 7 different years near the Greenwich Meridian. Decorrelation lengths are only about one-third of the color swath widths, so comparisons are difficult except in areas where repeat stations have been obtained.

lar, they provide insights and constraints on the system's ability to grow ice, the rates and limits of ice growth, and the influence of ice growth/melt on the ocean stability and heat flux. The absolute values of the parameters vary within relatively large (≤30%) intrinsic uncertainties, many owing to a lack of sufficient data, but their relative distributions show a good spatial signal to local noise ratio (~20 db). As such, the climatological maps of the parameters provide some intriguing relationships and patterns within the Weddell gyre where these general relationships have been applied. Specifically:

(1) The upper ocean freshwater content, controlled predominantly by the overlying ice dynamics and thermodynamics, and the upper ocean heat distribution, controlled predominantly by the large scale gyre dynamics and deep water characteristics, dictate the maximum amount of *in situ* ice growth and growth rates throughout the Weddell gyre region. Regarding thickness (growth rates are considered in point 4 below), it is seen from the summer salt deficit (Plate 13), that the fall ice growth, that is, the thickness of ice that grows rapidly in fall while eliminating the seasonal pycnocline prior to the onset of winter conditions, is typically 0.6 m or less. It is thinner than 0.3 m in some regions near the gyre core. This 0.3-0.6 m of ice can grow rapidly each fall since the seasonal pycnocline buffers the surface from the warm ocean deep water. Once the summer pycnocline is eliminated by this growth, the freshwater and heat content of the upper ocean during winter limits the ability of the water column to supporting only 0.5-1.0 m of additional winter ice growth throughout much of the gyre core (bulk stability; Plate 6). There are large regions, however, that can support another 1-3 m of growth before destabilizing the water column. If this maximum growth is exceeded, as has happened in the past as evidenced by the Weddell polynya, the water column will overturn and the resulting mode change cannot support an ice cover until the water column is eventually restabilized by a significant influx of freshwater at the surface.

(2) One of the most interesting results is that on regional scales, the ocean-ice system manages to vent the deep water at an average winter rate of 25-35 W m^{-2} throughout the gyre (Plate 11), regardless of the large scale stratification and dynamic setting. That is, despite the fact that the turbulent diffusive ocean heat flux varies by over an order of magnitude throughout the gyre (Plate 9), and the ocean entrainment heat flux varies by just under an order of magnitude (Plate 10), their sum, representing the net ocean sensible heat flux, only varies by ~30% across the gyre.

This predominantly indicates that where the pycnocline is relatively thick and the diffusive heat flux correspondingly weak, ice growth, unencumbered by a strong ocean heat flux, drives static instability due to salinization of the water column, which in turn drives an entrainment heat flux by eroding the weak pycnocline (whose enthalpy is replenished later via diffusion). The erosion may also be accomplished by storm-induced mixing (not associated with ice growth).

Alternatively, where the deep waters are close to the surface due to upwelling or the surface waters are close to the deep waters by storm mixing, the thermocline is stronger and more resistant to erosion and heat release via entrainment, but it provides a considerably higher diffusive flux to accomplish a similar magnitude venting. Furthermore, where the diffusive flux is larger, ice growth is reduced so the entrainment heat flux is further inhibited by weaker salinization-induced destabilization.

The diffusive and entrainment fluxes have complementary dependencies, so the system is ultimately successful in extracting the 25-35 W m^{-2} from the deep water regardless of which process dominates. Some of this spatial homogeneity in total ocean heat flux may be the result of using a spatially-invariant eddy diffusivity coefficient for estimating the diffusive heat flux, and assuming a spatially-invariant air-sea heat flux when computing the entrainment heat flux.

(3) Intense mixing due to the passage of intense polar lows may serve to reduce the bulk stability of the water column by as much as 75% (Plates 6 and 7) by venting the stabilizing heat contained within the thermocline independently of free convection driven by salinization during ice growth. This decouples the ice growth destabilization from the entrainment ocean heat flux. Also, storms may contribute to the particularly thin pycnocline in the eastern portion of the gyre, which enhances the ocean's diffusive heat flux, but reduces the ability of the ocean to resist ice growth through the negative feedback mechanism in which the ocean heat flux is increased by entrainment driven by salinization during ice growth.

(4) The large enthalpy content of the thermocline throughout most of the Weddell gyre region effectively reduces the ability to grow ice by a factor of 2-6 (see Plate 8). That is, the ice grows at a rate 2-6 times slower than expected by only considering the surface heat loss and ocean diffusive heat flux. Also, in the regions where the ice melt to growth rate ratio exceeds one, especially where it is considerably higher than one, we might expect long periods of significant melting. This basal melting may lead to negative ice freeboard given the weight of the snow on the ice, and thus these

regions where the ice melt to growth ratio exceeds one may correspond with regions in which ice flooding by seawater is most prevalent.

(5) Most of the bulk stability of the water column (given as the maximum amount of winter ice growth) is attributed to the enthalpy content of the thermocline (Plate 7), not by direct reduction in ice growth by a strong diffusive heat flux. That is, the majority of the ocean heat flux appears to originate from either entrainment driven by storms, or entrainment driven by ice growth. In both cases, the entrainment releases the enthalpy stored within the thermocline, which then acts to melt existing ice or to inhibit additional ice growth. This form of stabilization involves a more active ice growth-melt cycling since ice growth drives the ocean heat flux which drives ice melt, etc. In regions dominated by a diffusive heat flux, the ocean heat simply reduces the rate of ice growth and the entrainment heat flux is relatively minor because of the strong pycnocline.

The entrainment heat flux, when driven by ice growth, is the mechanism by which ocean sensible heat is vented to the atmosphere even when the surface layer is initially at the freezing point and thus can only give up heat in the form of latent heat of fusion. This latent heat loss must generate ice growth which drives entrainment, releasing sensible heat stored within the permanent thermocline. The results here suggest that the entrainment heat flux dominates the total ocean heat flux.

(6) Perturbations in the annual *in situ* ice growth of $\geq$80% are required to destabilize the water column throughout much of the Weddell gyre where summer data are available. However, these estimates are based on a small summer sample size. The likelihood of perturbations of such size in any one particular year must be estimated from more extensive multi-year sampling.

Finally, the bulk parameters presented here involve vertically-integrated property distributions, and, as such, they provide constraints or limitations on the ocean-ice system behavior over the appropriately averaged time scale — in this case, seasonal time scales. Consequently, they imply a mean seasonal evolution which may be considerably different from the actual time-dependent behavior. Also, they must still be diagnosed against complete models and modified to include any relevant nonlinear physics influencing the mean behavior. Some attempt was made to estimate the important influence of storms in this analysis. In general, the parameters serve to demonstrate the extent to which fairly fundamental characteristics of the OAI system may be extracted from simple-to-observe features of the water column. Additional temporal coverage is required to ultimately determine the distributions, allowing assessment of the likelihood of destabilization in the system and significant change in the ocean-ice behavior.

Because the parameters discussed here represent physically meaningful combinations of the water column features, these, or other such combinations, may represent more physically meaningful (and sensitive) diagnostics for model-data comparison than profile shapes or individual property values.

Acknowledgments. Special thanks to Karen Heywood, Eberhard Fahrbach and Michael Schroeder for making their CTD data readily available for this study, and to Christoph Kottmeier for making his buoy data available. This work was supported by National Science Foundation research grant OPP93-17231. Lamont-Doherty Earth Observatory contribution number 5690.

REFERENCES

Ackley, S.F., M. Lange and P. Wadhams, Snow cover effects on Antarctic sea ice thickness. In, *Sea Ice Properties and Processes*: Proc. of the W.F. Weeks Symposium, S.F. Ackley and W.F. Weeks, eds., CRREL Monograph 90-1, 16-21, 1990.

Akitomo, K., T. Awaji and N. Imasato, Open-ocean deep convection in the Weddell Sea: two-dimensional numerical experiments with a nonhydrostatic model, *Deep-Sea Res.*, 42, 53-73, 1995.

Bagriantsev, N.V., A.L. Gordon, and B.A. Huber, Weddell Gyre: Temperature maximum stratum, *J. Geophys. Res.*, 94, 8331-8334, 1989.

Bersch, M., G.A. Becker, H. Frey, K.P. Koltermann, Topographic effects of Maud Rise on the stratification and circulation of the Weddell Gyre, *Deep Sea Res.*, 303-331, 1992.

Eicken, H., and M.A. Lange, Development and properties of sea ice in the coastal regime of the southeastern Weddell Sea, *J. Geophys. Res.*, 94, 8193-8206, 1989.

Foldvik, A. and T. Gammelsrod, Notes on Southern Ocean hydrography, sea-ice and bottom water formation, *Palaeogeogr., Palaeoclimatol., Palaeoecol.*, 67, 3-17, 1988.

Garwood, R.W., Jr., S.M. Isakari and P.C. Gallacher, Thermobaric convection, in *The Polar Oceans and Their Role in Shaping the Global Environment*, Johannessen, Muench and Overland (eds.), Geophys. Monogr. 85, 199-209, 1994.

Gordon, A.L., Deep Antarctic convection west of Maud Rise, *J. Phys. Oceanogr.*, 8, 600-612, 1978.

Gordon, A.L., Seasonality of Southern Ocean sea ice, *J. Geophys. Res.*, 85, 4193-4197, 1981.

Gordon, A.L., Two stable modes of Southern Ocean winter stratification, in *Deep Convection and Deep Water Formation in the Oceans*, eds. Chu and Gascard, Elsevier Science Publishers, 17-35, 1991.

Gordon, A.L. and B.A. Huber, Thermohaline stratification below the Southern Ocean sea ice, *J. Geophys. Res.*, 89, 641-648, 1984.

Gordon, A.L., and B.A. Huber, Southern Ocean winter mixed layer, *J. Geophys. Res.*, 95, 11655-11672, 1990.

Gordon, A.L., B.A. Huber, H.H. Hellmer and A. Ffield, Deep and bottom water of the Weddell Sea's western rim, *Science*, 262, 95-97, 1993.

Gordon, A.L. and E.J. Molinelli, Southern Ocean Atlas: Thermohaline and Chemical Distributions and the Atlas Data Set, International Decade of Ocean Exploration, Columbia University Press, 1982.

Gregg, M.C., The dependence of turbulent dissipation on stratification in a diffusively stable thermocline, *J. Geophys. Res.*, 93, 12381-12392, 1988.

Hansen, J., A. Lacis, D. Rind, G. Russell, P. Stone, I. Fung, R. Ruedy, and J.Lerner, Climate sensitivity: analysis of feedback mechanisms. *Climate Processes and Climate Sensitivity*, Geophys. Monogr. 29, Maurice Ewing Volume 5, American Geophysical Union, 130-163, 1984.

Heywood, K.J. and B.A. King, WOCE section A23 Cruise Report, Series No. 1, Southampton Oceanography Center, University of East Anglia, Norwich, 75 pp, 1996.

Imbrie, J., E.A. Boyle, S.C. Clemens, A. Duffy, W.R. Howard, G. Kukla, J. Kutzbach, D.G. Martinson, A. McIntyre, A.C. Mix, B. Molfino, J.J. Morley, L.C. Peterson, N.G. Pisias, W.L. Prell, M.E. Raymo, N.J. Shackleton, and J.R. Toggweiller, On the structure and origin of major glaciation cycles. 1. Linear responses to Milankovitch forcing. *Paleoceanography*, 7,6, 701-738, 1992.

Jacobs, S.S., H.H. Hellmer, C.S.M. Doake, A. Jenkins and R.M. Frolich, Melting of ice shelves and the mass balance of Antarctica, *J. Glaciology*, 38, 1992.

Killworth, P.D., On "chimney" formations in the ocean, *J. Phys. Oceanogr.*, 9, 531-554, 1979.

Kottmeier, C., S. Ackley, E. Andreas, D. Crane, H. Hoeber, J. King, J. Launiainen, D. Limbert, D. Martinson, R. Roth, L. Sellmann, P. Wadhams and T. Vihma, Wind, temperature and ice motion statistics in the Weddell Sea, World Climate Research Programme, International Programme for Antarctic Buoys, WMO/TD-No.797, 1997.

Ledley, T.S., The climatic response to meridional sea-ice transport, *J. Climate*, 4, 147-163, 1991.

Ledwell, J.R., A.J. Watson and C.S. Law, Evidence for slow mixing across the pycnocline from an open-ocean tracer-release experiment, *Nature*, 364, 701-703, 1993.

Manabe, S., R. J. Stouffer, M.J. Spelman and K. Bryan, Transient responses of a coupled ocean-atmosphere model to gradual changes of atmospheric CO_2. Part I: Annual mean response. *J. of Climate*, 4, 785-818, 1991.

Martinson, D.G., P.D. Killworth, A.L. Gordon, A convective model for the Weddell polynya, *J. Phys. Oceanogr.*, 11, 466-488, 1981.

Martinson, D.G., Evolution of the Southern Ocean winter mixed layer and sea ice; open ocean deepwater formation and ventilation, *J. Geophys. Res.*, 95, 11641-11654, 1990.

Martinson, D.G., Ocean heat and seasonal sea ice thickness in the Southern Ocean, NATO ASI Series, Vol. I, Ice in the Climate System, ed. W. Richard Peltier, Springer-Verlag, 1993.

McPhee, M.G., S.F. Ackley, P. Guest, B.A. Huber, D.G. Martinson, J.H. Morison, R.D. Muench, L. Padman, T.P. Stanton, The Antarctic Zone Flux Experiment, *Bull. Amer. Met. Soc.*, 77, 1221-1232, 1996.

Meehl, G.A. and W.M. Washington, CO_2 climate sensitivity and snow-sea-ice albedo parameterization in an atmospheric GCM coupled to a mixed-layer ocean model, *Climate Change*, 16, 283-306, 1990.

Motoi, T., N. Ono and M. Wakatsuchi, A mechanism for the formation of the Weddell polynya in 1974, *Am. Meteorol. Soc.*, 17, 2241-2247, 1987.

Orsi, A.H., T.I. Whitworth and W.D.J. Nowlin, On the meridional extent and fronts of the Antarctic Circumpolar Current, *Deep Sea. Res.*, 42, 641-673, 1995.

Parkinson, C.L., On the development and cause of the Weddell polynya in a sea ice simulation, *J. Phys. Oceanogr.*, 13, 501-511, 1983.

Rind, D., R. Healy, C. Parkinson and D. Martinson, The role of sea ice in $2XCO_2$ climate model sensitivity. Part I: The total influence of sea ice thickness and extent, *Amer. Meteorol. Soc.*, 1-15, 1995.

Schlesinger, M., and J. Mitchell, Model projections of the equilibrium climatic response to increased carbon dioxide, in *The Potential Climatic Effects of Increasing Carbon Dioxide*, DOE/ER-0237, 81-148, U.S. Dept. of Energy, 1985.

Schlosser, P., W. Roether and G. Rohardt, ^{3}He balance of the upper layers of the northwestern Weddell Sea, *Deep-Sea Res.*, 34, 365-377, 1987.

Sellmann, L., and Ch. Kottmeier, Sea ice buoys 1991 - 1995 data documentation, Alfred-Wegener-Institut für Polar- und Meeresforschung, *Berichte aus dem Fachbereich Physik*, 1996.

Smith, W.H.F. and P. Wessel, Gridding with continuous curvature splines in tension, *Geophys.*, 55, 293-305, 1990.

Wadhams, P., M.A. Lange and S.F. Ackley, The ice thick-

ness distribution across the Atlantic sector of the Antarctic Ocean in midwinter, *J. Geophys. Res.*, 92, 14535-14552, 1987.

Wadhams, P., Sea ice thickness changes and their relation to climate, In: *The Polar Oceans and Their Role in Shaping the Global Environment*, eds., Johannessen, Muench and Overland, Geophys. Monogr., 337-361, 1994.

Walin, G., On the formation of ice on deep weakly stratified water, *Tellus*, 45A, 143-157, 1993.

Washingon, W.M. and G.A. Meehl, Seasonal cycle experiment on the climate sensitivity due to a doubling of CO_2 with an atmospheric general circulation model coupled to a simple mixed-layer ocean model, *J. Geophys. Res.*, 89, 9475-9503, 1984.

Wessel, P. and W.H.F. Smith, Free software helps map and display data, *EOS Trans. Amer. Geophys. U.*, 72, 441, 445-446, 1991.

Zwally, H.J. and Gloersen, P., Passive microwave images of the polar regions and research application, *Polar Rec.*, 18, 431-450, 1977.

Douglas G. Martinson and Richard A. Iannuzzi, Lamont-Doherty Earth Observatory, and Department of Earth and Environmental Sciences, Columbia University, Palisades, NY 10964

(Received October 29, 1996;
accepted August 14, 1997.)